OPTIMAL PLACEMENT OF DAMPERS IN STRUCTURES BASED ON TARGET-ORIENTED KRILL HERD ALGORITHM

Dissertation

Presented to Faculty of Engineering,
Kanagawa University in Partial Fulfillment of the Requirements for
the Degree of Doctor of Engineering

Submitted by

Lixiang Cheng

Supervised by

Professor **Kazushi Shimazaki**

CONTENTS

ABSTRACT

During a seismic event, ground movement transfers a massive amount of energy to structures; even comparatively weak seismic motions may result in tremendous constructive damage and many fatalities. To reduce inelastic energy dissipation demand on the framing system of structures, viscous dampers (VDs) are used in new structures as well as the deficient structures due to its adaptability, easy installation, and simple design. The use of VDs reduces damage to the frame systems, and where the VDs are positioned in the structure directly affects its seismic performance. In particular, high-rise structures offer more options for damper placement, so it is necessary to find an appropriate method for placing dampers optimally in a structure.

The krill herd (KH) algorithm is widely used in engineering optimization as no gradient information is necessary, and only a few parameters require adjustment. However, in high-rise structures, when dampers can place in many locations, KH often falls into local optimality. Therefore, this study proposes a novel target-oriented krill herd (TOKH) algorithm to solve complex engineering optimization problems. Especially the optimal placement of dampers in high-rise buildings. The following main conclusions are drawn:

1). The time complexity experiment performed using the Rastrigin benchmark function demonstrated that the running time of TOKH algorithm was linear based on the number of iterations, which was consistent with the inference of big-O. The two operators introduced do not change the time complexity of TOKH.

2). TOKH algorithm was compared with nine other algorithms using 15 benchmark functions. The performance of TOKH algorithm for most functions and different dimensions, particularly for different types of high-dimensional functions, was statistically superior to those of the other metaheuristic algorithms.

3). TOKH algorithm was applied to four discrete truss optimization problems under multiple loading conditions. We compared the numerical results for various trusses obtained using TOKH algorithm with other methods in the literature to verify the effectiveness, efficiency, and robustness. The results indicated that, among the ten algorithms, TOKH algorithm is competitive in terms of optimal weight, average weight, and stability. Furthermore, TOKH algorithm demonstrated significantly faster convergence to the optimal solution compared to other methods. Compared to KH algorithm, although TOKH required slightly more computational cost, its optimization

efficiency improved by 20.90, 17.37, 53.53, and 88.01%, respectively. As the complexity of the truss increased, the advantage of TOKH became more evident. The proposed TOKH algorithm can serve as an ideal method for handling discrete truss problems.

4). The high-rise structural example indicate that compared with other algorithms, the VD locations found by TOKH algorithm give better seismic performance. Meanwhile, the TOKH also has good global convergence.

5). The VD placements obtained by TOKH are mainly in the middle and lower stories of the high-rise structure, which is consistent with practical experience.

6). TOKH offers a practical and powerful method for determining the optimal damper placement in high-rise structures.

Keywords: Viscous damper, Optimal placement, Discrete truss optimization, Target-oriented, Krill herd algorithm, Robustness.

概要

地震時には、地面の動きが構造物に大量のエネルギーを伝達し、比較的弱い地震動でも膨大な建造物の損傷や多くの死者を引き起こす可能性があります。構造物の枠組みシステムへの非弾性エネルギー散逸要求を減少させるために、新しい構造物や不足している構造物には、適応性が高く、取り付けが容易で、設計がシンプルな粘性ダンパー（VD）が使用されています。VD の使用により、フレームシステムの損傷が減少し、VD が構造物内でどのように配置されているかが、その地震性能に直接影響します。特に、高層建築物では、ダンパーの配置オプションが多いため、構造物内で最適にダンパーを配置する適切な方法を見つけることが必要です。

クリルハード（KH）アルゴリズムは、勾配情報が不要で、調整が必要なパラメータが少ないため、工学最適化で広く使用されています。しかし、高層建築物でダンパーを多くの場所に配置できる場合、KH はしばしば局所最適性に陥ります。したがって、本研究では、複雑な工学最適化問題を解決するための新しい目標指向クリルハード（TOKH）アルゴリズムを提案します。特に高層ビルでのダンパーの最適配置についてです。以下の主な結論が導かれました：

1). ラストリギンベンチマーク関数を使用した時間複雑性実験により、TOKH アルゴリズムの実行時間は反復回数に基づいて線形であることが示され、これは big-O の推論と一致しています。導入された 2 つのオペレータは、TOKH の時間複雑性を変更しません。

2). TOKH アルゴリズムは、15 のベンチマーク関数を使用して他の 9 つのアルゴリズムと比較されました。TOKH アルゴリズムの性能は、ほとんどの関数と異なる次元、特に異なるタイプの高次元関数に対して、他のメタヒューリスティックアルゴリズムよりも統計的に優れていました。

3). TOKH アルゴリズムは、複数の荷重条件下で 4 つの離散トラス最適化問題に適用されました。文献の他の方法を使用して得られた様々なトラスの数値結果と比較して、効果、効率、および堅牢性を検証しました。その結果、10

のアルゴリズムの中で、TOKH アルゴリズムは最適重量、平均重量、および安定性の点で競争力があります。さらに、TOKH アルゴリズムは他の方法と比較して最適解への収束が著しく速かった。KH アルゴリズムと比較して、TOKH はわずかに多くの計算コストが必要でしたが、その最適化効率はそれぞれ 20.90、17.37、53.53、および 88.01%向上しました。トラスの複雑さが増すにつれて、TOKH の利点がより明らかになりました。提案された TOKH アルゴリズムは、離散トラス問題を取り扱うための理想的な方法として機能します。

4). 高層建築物の例では、他のアルゴリズムと比較して、TOKH アルゴリズムによって見つかった VD の位置は、地震性能が良好であることが示されました。同時に、TOKH は良好な全体収束も持っています。

5). TOKH によって得られた VD 配置は、主に高層構造物の中間および下層階にあり、これは実践的な経験と一致しています。

6). TOKH は、高層構造物におけるダンパー配置の最適化を決定するための実用的かつ強力な方法を提供します。

CHAPTER 1. INTRODUCTION

1.1 Research background

During a seismic event, ground movement transfers a massive amount of energy to structures; even comparatively weak seismic motions may result in tremendous constructive damage and many fatalities [1]. To reduce inelastic energy dissipation demand on the framing system of structures, viscous dampers (VDs) are used in new structures as well as the deficient structures [2]. The use of VDs reduces damage to the frame systems, and where the VDs are positioned in the structure directly affects its seismic performance [3]. In particular, high-rise structures offer more options for damper placement, so it is necessary to find an appropriate method for placing dampers optimally in a structure [4-5]. VDs distribution methods have been recommended for response reduction in structures, and dampers can be located along the height of a building by three approaches: analytical, heuristic, and evolutionary (metaheuristic) methods, respectively [6]. Of these, the metaheuristic approach is receiving increasing attention because of its easy implementation, parallel computing, and absence of gradient calculations [7], and some examples of this approach are given below.

Apostolakis and Dargush [8] established a computational method on the basis of genetic algorithm (GA) for the hysteretic passive dampers design inside steel moment-resisting frames. Furthermore, the computational framework explored the optimum locations for relinquishing metallic buckling restrained braces and moment-resisting frames.

Sarcheshmehpour et al. [9] determined the optimal location of dampers for 2D steel moment frames by GA to satisfy three levels of service performance, life safety, and collapse prevention as target performance. The endurance time method was utilized for the frames analysis and seismic response estimation. Results show that the maximum drift ratio reduction is obtained at low excitation intensities; however, less drift is calculated in the upper floors of the fixed-based frames in comparison with the soil-structure systems.

Bogdanovic and Rakicevic [10] performed the optimization process of damper placement by GA and thirty optimum solutions were concluded. Without optimization, the process is complex and takes a long computational time to achieve the required

solutions but considering the reduction in drifts and acceleration as objective functions, leads to better structural performance for optimum damper placement.

Sonmez et al. [11] presented and utilized artificial bee colony (ABC) algorithm to optimize the location and size of VDs in planar buildings, which effectively increase the resistance of frame systems to earthquakes. For a planar building frame, the design variables were the damper coefficients and objective function was defined as the elastic base shear force and the top displacement transfer function amplitude. The presented technique is proved by considering the steepest direction search algorithm. The ABC algorithm is a relatively simple method to solve the damper configuration issue.

Amini and Ghaderi [12] developed a hybridized search algorithm named Ant Harmony Search (AntHS) for combinatorial optimization problems and in particular for finding optimal locations of dampers in a structural system. Based on numerical examples the idea of a dynamic probability mass function helps the AntHS to identify potentially qualified areas in the search space faster while avoid stagnation and being trapped in local optima.

Miguel et al. [13] studied a technique that performs efficiently to discover the optimum design for both placement and force of dampers located in the footbridges. This was achieved by implementing the firefly algorithm (FA). Two footbridges were analyzed, considering the positions and forces of the friction dampers as the design variables, and minimizing the maximum acceleration as the cost function. This method was useful in determining both the optimal friction force and the ideal location of each damper.

Çerçevik et al. [14] used two metaheuristic algorithms (the bat algorithm and the dragonfly algorithm) for position optimization to find the minimum number of dampers subject to the specified limits for the peak floor acceleration and inter-story drift ratios. Using these approaches, they managed to place the fewest dampers in the most suitable spans.

Ayyash and Hejazi [15] hybridized the particle swarm optimization (PSO) and gravitational search algorithm (GSA) to optimize the performance of earthquake energy dissipation systems (i.e., damper devices) simultaneously with optimizing the characteristics of the structure. To examine the performance of the proposed PSO-GSA optimization method, it was applied to a three-story reinforced structure

equipped with a seismic damper. The results revealed that the method successfully optimized the earthquake energy dissipation systems and reduced the effects of earthquakes on structures, which significantly increase the building's stability and safety during seismic excitation.

The above metaheuristic algorithms have been extensively used for optimally placing dampers in structures. However, high-rise buildings subjected to seismic excitation exhibit stronger dynamic responses, and there is an urgent need to find the optimal location of dampers in such buildings [16]. Unfortunately, as the number of structural stories increases, so does the number of damper placement combinations, which in turn places higher demands on the global optimization performance of existing metaheuristic algorithms.

The target-oriented krill herd (TOKH) algorithm is an improved krill herd (KH) algorithm that is both robust and competitive. Compared with other metaheuristic algorithms, TOKH shows stronger global optimization performance, and its robustness has been verified by benchmark functions and structural reliability analysis. In this paper, the TOKH algorithm is proposed to solve the optimal placement of VDs in high-rise structures. The effectiveness of TOKH is evaluated using a 22-story shear building and a 20-story frame structure [17], and the results show that its damper placement gives seismic performance that is more efficient than that obtained with other methods in the literature.

1.2 Objectives and organization

The objectives of this dissertation would be:

(1). To optimize the damper placement in high-rise structures, a TOKH algorithm is proposed.

(2). The robustness of the proposed TOKH algorithm is verified by benchmark function and truss optimization, and it is applied to the optimal placement of dampers in high-rise structures.

For the purpose, four chapters will be covered in this dissertation. The organization is given as follows:

In chapter two, the implementation principle of the TOKH algorithm is introduced in detail, and the robustness of TOKH in solving discrete optimization problems is verified through benchmark function and truss optimization examples.

In chapter three, the optimization performance of TOKH in the damper placement of high-rise structures is verified through three damper optimization placement examples.

In chapter four, the conclusions will be summarized.

References

[1] B.Gencturk, K.Hossain, and S.Lahourpour: Life cycle sustainability assessment of RC buildings in seismic regions, Engineering structures, Vol.110, pp.347-362, 2016.

[2] D.De Domenico, G.Ricciardi, and I.Takewaki: Design strategies of viscous dampers for seismic protection of building structures: a review, Soil dynamics and earthquake engineering, Vol.118, pp.144-165, 2019.

[3] J.K.Whittle, M.S.Williams, T.L.Karavasilis, and A.Blakeborough: A comparison of viscous damper placement methods for improving seismic building design, Journal of Earthquake Engineering, Vol.16, pp.540-560, 2012.4.

[4] R.J.Mcnamara, and D.P.Taylor: Fluid viscous dampers for high-rise buildings, The structural design of tall and special buildings, Vol.12, pp.145-154, 2003.2.

[5] Y.Nurchasanah, and M.L.Harnadi: Assessment of Viscous Damper Placement as Passive Energy Dissipation on High-rise Building, a Numerical Study, In Journal of Physics: Conference Series, Vol.1858, p.012096, 2021.4.

[6] D.L.Garcia: A simple method for the design of optimal damper configurations in MDOF structures, Earthquake spectra, Vol.17, pp.387-398, 2001.3.

[7] D.Caicedo, L.Lara-Valencia, J.Blandon, and C.Graciano: Seismic response of high-rise buildings through metaheuristic-based optimization using tuned mass dampers and tuned mass dampers inerter, Journal of Building Engineering, Vol.34, p.101927, 2021.

[8] G.Apostolakis, and G.F.Dargush: Optimal seismic design of moment-resisting steel frames with hysteretic passive devices, Earthquake engineering & structural dynamics, Vol.39, pp.355-376, 2010.4.

[9] M.Sarcheshmehpour, H.E.Estekanchi, and M.A.Ghannad: Optimum placement of supplementary viscous dampers for seismic rehabilitation of steel frames considering soil–structure interaction, The Structural Design of Tall and Special Buildings, Vol.29, p.e1682, 2020.1.

[10] A.Bogdanovic, and Z.Rakicevic: Optimal damper placement using combined fitness function, Frontiers in Built Environment, Vol.5, p.4, 2019.

[11] M.Sonmez, E.Aydin, and T.Karabork: Using an artificial bee colony algorithm for the optimal placement of viscous dampers in planar building frames, Structural and Multidisciplinary Optimization, Vol.48, pp.395-409, 2013.

[12] F.Amini, and P.Ghaderi: Hybridization of harmony search and ant colony optimization for optimal locating of structural dampers, Applied Soft Computing, Vol.13, pp.2272-2280, 2013.5.

[13] L.F.F.Miguel, L.F.Fadel Miguel, and R.H.Lopez: A firefly algorithm for the design of force and placement of friction dampers for control of man-induced vibrations in footbridges, Optimization and Engineering, Vol.16, pp.633-661. 2015.

[14] A.E.Çerçevik, Ö.Avşar, and A.Dilsiz: Optimal placement of viscous wall dampers in RC moment resisting frames using metaheuristic search methods, Engineering Structures, Vol.249, p.113108, 2021.

[15] N.Ayyash, and F.Hejazi: Development of hybrid optimization algorithm for structures furnished with seismic damper devices using the particle swarm optimization method and gravitational search algorithm, Earthquake Engineering and Engineering Vibration, Vol.21, pp.455-474, 2022.2.

[16] L.Suresh, and K.M.Mini: Effect of multiple tuned mass dampers for vibration control in high-rise buildings, Practice Periodical on Structural Design and Construction, Vol.24, p.04019031, 2019.4.

[17] Y.Ohtori, R.E.Christenson, B.F.Spencer Jr, and S.J.Dyke: Benchmark control problems for seismically excited nonlinear buildings, Journal of engineering mechanics, Vol.130, pp.366-385, 2004.4.

CHAPTER 2. TARGET-ORIENTED KRILL HERD (TOKH) ALGORITHM

Truss optimization has gained considerable attention because of its direct applicability to the design of structures. Designers and owners require optimized trusses to reduce building costs [1]. However, the implementation of discrete truss optimization problems is challenging as several truss designs generally entail a complex design space. Traditionally, researchers have used mathematical approaches that employ rounding off techniques based on continuous solutions to solve discrete truss optimization problems. However, these methods may become infeasible or generate increasingly suboptimal solutions with numerous variables [2]. Therefore, simulation-based metaheuristic algorithms to solve truss optimization problems are required.

Metaheuristic algorithms combine rules and randomness to imitate natural phenomena and attempt to identify the optimum design in a reasonable amount of computing time using trial-and-error techniques [3]. The ability to balance exploitation (intensification) and exploration (diversification) during a search determines the efficiency of a specific metaheuristic algorithm. Exploration ensures the validity and breadth of the algorithm in the search area, which can be beneficial for global optimization. Exploitation expands the local search for the currently explored optimal area and further finds the minimum [4]. To address global search requirements, modern metaheuristic algorithms have evolved to incorporate three primary purposes, namely, solving problems faster, solving larger problems, and enhancing algorithm robustness [4]. Modern metaheuristic algorithms include the genetic algorithm (GA) [5–7], biogeography-based optimization [8–10], harmony search (HS) [11–13], differential evolution [14, 15], ant colony optimization [16], particle swarm optimization [17–19], artificial bee colony [20–22], teaching-learning based optimization (TLBO) [23], artificial fish swarm [24], firefly algorithm [25–27], political optimizer (PO) [28], cuckoo search [29, 30], bat algorithm [31, 32], manta ray foraging optimization (MRFO) [33] and krill herd (KH) algorithm [34]. Among these algorithms, the KH algorithm is known for its powerful exploitation ability, adjustment of fewer parameters, and easy implementation.

The KH algorithm was inspired by the herding behavior of Antarctic krill swarms. During optimization, each krill is primarily affected by other krill individuals, foraging action, and physical diffusion. Foraging and other krill-induced motions include two global and two local strategies that operate in parallel, rendering KH a robust algorithm [34]. Compared to earlier metaheuristic algorithms, the KH algorithm imposes fewer mathematical requirements and can be easily adapted to solve various engineering optimization problems. Furthermore, rather than using a gradient search, the KH algorithm uses a stochastic search based on the krill population, which eliminates the need for derivative information. These features have increased the flexibility of the KH algorithm and produced better solutions. Consequently, it has been increasingly investigated and successfully employed in various practical structural optimization problems, such as truss structures [35], pin-jointed plane frames [36], and welded beams [37].

Nevertheless, the KH algorithm can cause a risk of stagnancy after the initial stage when applied to multi-extreme discrete optimization problems. Therefore, several approaches have been explored to increase the diversity of solutions, resulting in a few KH variations with improved performance. A chaotic KH (CKH) algorithm was presented to improve global optimization [38], wherein the three primary movements of a krill swarm were adjusted during the optimization process using various chaotic maps. An opposition KH (OKH) algorithm was proposed to increase the diversity of the population [39]. Herein, three operators, namely, opposition-based learning, position clamping, and Cauchy mutation were added to the normal KH algorithm to improve the global convergence. A multi-stage KH (MSKH) algorithm was introduced in [40] by adding a local mutation and crossover operator and an elite scheme in the exploitation stage. This resulted in the complete utilization of the global and local search capabilities of the krill swarm to solve the global numerical optimization problem. Guo et al. [41] proposed an improved KH (IKH) algorithm, wherein information could be exchanged between the top krill during movement. The IKH algorithm employed a novel Lévy flight distribution to extend the search range and added an elite scheme to update the krill-motion calculation, generate better candidate solutions, and accelerate global convergence. Laith et al. [42] proposed a modified KH algorithm (MKHA) to improve global exploration by modifying the genetic operator of the basic KH. After analyzing the influence of a step-size scaling

factor *ct* on KH, Li et al. [43] advanced KH with a linear decreasing step (KHLD), wherein *ct* was linearly decreased over time to balance exploration and exploitation. Another study [44] used stud KH (SKH) algorithm for 22 benchmark functions. Furthermore, a levy-flight KH (LKH) algorithm [45] was proposed to improve the optimization performance of the KH algorithm; its effectiveness was verified using several benchmark functions.

Although several variants of KH algorithm enhance its optimization performance, their accuracy when handling discrete truss optimization problems remains unsatisfactory. The aforementioned algorithms ignore the effect of the "suboptimal krill" and "center of food" on the aggregation of KH, resulting in an inadequate balance between global exploration and local exploitation. Typically, the discrete truss optimization easily falls into a local minimum. To prevent this, a novel target-oriented KH (TOKH) algorithm is proposed in this study, which considers both the "suboptimal krill" and "center of food". Initially, the "suboptimal krill" and "best krill" were crossed to generate a novel "cross krill" for better global exploration. Subsequently, an improved local mutation and crossover (ILMC) operator was applied to fine-tune the "center of food" and population to improve local exploitation for effectively solving truss optimization. Four discrete truss design problems are applied to verify the robustness of the developed TOKH algorithm. The optimization efficiency of TOKH algorithm increased by 20.90, 17.37, 53.53 and 88.01% for the four problems when compared to those of KH algorithm. The results verify that the proposed method is highly competitive with other optimization approaches reported in the literature and avoids falling into a local optimum.

2.1 The principle of TOKH

2.1.1 KH algorithm

This subsection briefly introduces the principles of KH [34] algorithm. KH algorithm uses an optimization process to attain a global solution defined using an objective function similar to the process by which a krill swarm obtains food and gathers continuously. Over time, the location of an individual krill is determined by three primary movements, namely,

i: Motion induced by other individuals,

ii: Foraging action, and

iii: Physical diffusion.

These motion types can be expressed using a Lagrangian model in a *n*-dimensional decision space as follows [34]:

$$\frac{dX_i}{dt} = N_i + F_i + D_i \tag{2.1}$$

where $\frac{dX_i}{dt}$ denotes the speed of each krill, and N_i, F_i, and D_i indicate the motions induced by other krill individuals, foraging action, and physical diffusion of the *i*-th krill individuals, which can be obtained using Eqs. (2.2), (2.4), and (2.6), respectively.

The approximate value of the direction of induced motion (α_i) can be calculated using a target swarm density (target effect), local swarm density (local effect), and repulsive swarm density (repulsive effect). For krill individual *i*, this movement can be formulated as [38]:

$$N_i^{new} = N^{max}\alpha_i + \omega_n N_i^{old} \tag{2.2}$$

where

$$\alpha_i = \alpha_i^{local} + \alpha_i^{target} \tag{2.3}$$

Here, N^{max} denotes the maximum induced speed, ω_n indicates the inertia weight of the motion induced in the range of [0,1], N_i^{old} represents the last motion induced, α_i^{local} and α_i^{target} denote the local and target effects, respectively.

The foraging action involves two primary components, namely, the current "center of food" location and previous experience with respect to the "center of food" position. The foraging action for the *i*-th krill can be expressed as follows [38]:

$$F_i = V_f\beta_i + \omega_f F_i^{old} \tag{2.4}$$

where

$$\beta_i = \beta_i^{food} + \beta_i^{best} \tag{2.5}$$

Here, V_f denotes the foraging speed, ω_f indicates the inertia weight within the range [0,1], β_i^{food} represents the "center of food" attraction, β_i^{best} denotes the effect of the best fitness, and F_i^{old} indicates the last foraging action.

The third part of physical diffusion is primarily affected by the maximum diffusion rate and random vector. The physical diffusion can be expressed as [38]:

$$D_i = D^{max}\delta \tag{2.6}$$

where D^{max} denotes the diffusion speed, and δ indicates a random vector within the range [−1,1].

Foraging actions and movements induced by other krill individuals involve two global and two local optimization strategies. The simultaneous operation of these optimization strategies renders the KH algorithm a powerful optimization method. During a specific period, different effective movement parameters of the movement can be used. The changes in the location of a krill individual from t to $t+\Delta t$ can be expressed as follows [34]:

$$X_i(t+\Delta t) = X_i(t) + \Delta t \frac{dX_i}{dt} \tag{2.7}$$

where Δt is an important parameter that completely depends on the search space. Here, Δt can be increased appropriately when the search space is wide, and when the search space is small, it can be appropriately reduced. Additionally, the crossover and mutation mechanisms of GA [5] can be incorporated to improve the performance of KH algorithm.

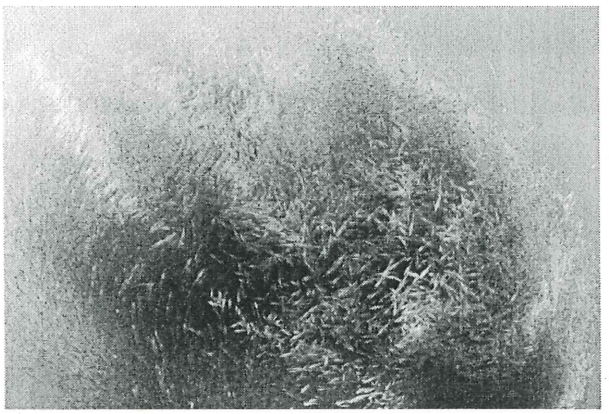

Fig. 2.1 Krill swarms in the ocean

2.1.2 Improvement operators

Local exploitation and global exploration are the two critical components of modern metaheuristic algorithms. Exploitation reinforces the local search for minimum or near-optimal solutions, whereas exploration involves a global search to ensure the efficient and effective exploration of the search space [4]. Excessive

diversification causes solutions to jump around from one potentially optimal solution to another, increasing the convergence time required to reach optimum. However, excessive reinforcement may trap the algorithm in local optimum, as only a portion of the local space may be visited. Therefore, an effective algorithm requires an appropriate balance between these two components to ensure efficient convergence, avoid falling into a local optimum, and guarantee the solution accuracy.

KH algorithm has demonstrated its ability to identify near-global regions in continuous-truss optimization problems [35]. However, the insufficient balance between global exploration and local exploitation causes the algorithm to easily fall into a local optimum when solving discrete truss optimization problems. The proposed TOKH algorithm intends to balance the associated exploitation and exploration components to solve the discrete truss optimization problem more efficiently.

This subsection describes the basic principle of TOKH algorithm. The learning efficiency of the population oriented to the "suboptimal krill" and "best krill" should be improved to enhance the global optimization of KH algorithm. In the exploration phase, a crossover operator was established between the "suboptimal krill" and "best krill" to generate a "cross krill". The crossover Lagrangian model can be expressed as

$$X_c = X_i + \omega \cdot (X_{best} - X_i) - \lambda \cdot (X_i - X_{sub}) \tag{2.8}$$

where X_c, X_i, X_{best}, and X_{sub} denote the "cross krill", "current krill", "best krill", and "suboptimal krill" respectively; and w and l indicate different random numbers in the range of [0,1]. If the fitness value of X_c was better than that of X_{best}, X_c was replaced by X_{best}. Algorithm 1 presents the pseudocode used to achieve the aforementioned crossover operator.

Algorithm 1 : Pseudocode of the crossover operator.

Begin

$X_c = X_i + w * (X_{best} - X_i) - l * (X_i - X_{sub})$

if X_c is better than X_{best} **then**

$X_{best} = X_c$

end if

End

Through the above cooperative strategy, the "cooperative krill" can further leverage valid information on "best krill" and "food" to conduct better searches in unknown areas, and to strike a balance between diversification and intensification. To intuitively feel the powerful effect of adding the "cooperative krill", the movement trajectories of the "best krill", "food", and "cooperative krill" are recorded using the unimodal Schwefel 2.22 function and the multimodal Rastrigin function. Fig. 2.2 manifests the three-dimensional graph of two functions. In the experiment on testing the motion trajectories of three particles, there are a total of 10 krill, 3 dimensions, and 50 iterations. The positions of the three particles iterations [1, 5, 15, 30, 50] are reported. The motion trajectories of the three particles are displayed in Fig. 2.3. It can be displayed clearly that during the iteration, the "best krill" has a larger range of motion (global exploration), and "food" has a smaller range of motion (local exploitation). The range of motion of the "cooperative krill" is between the "best krill" and "food", filling in the gap in the optimization space of two factors. The experiment result evinces that the cooperative strategy better balances global exploration and local exploitation.

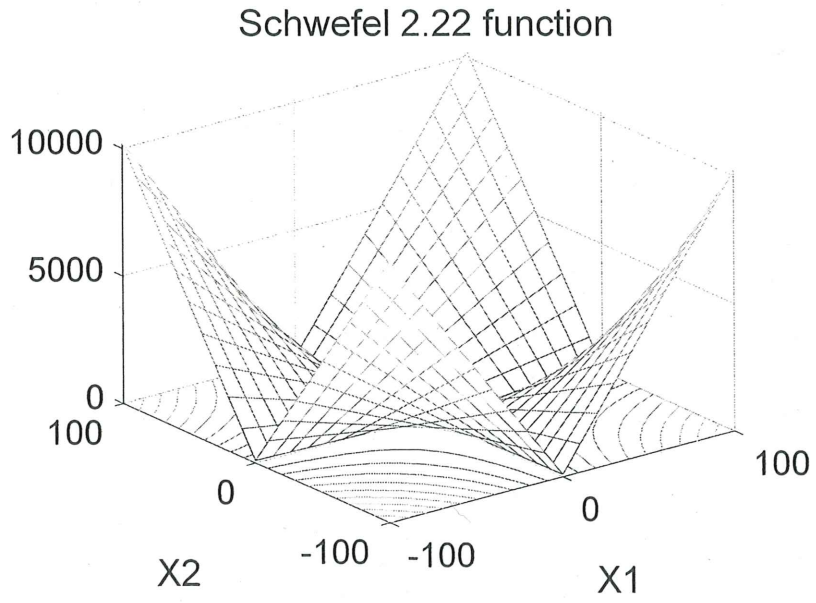

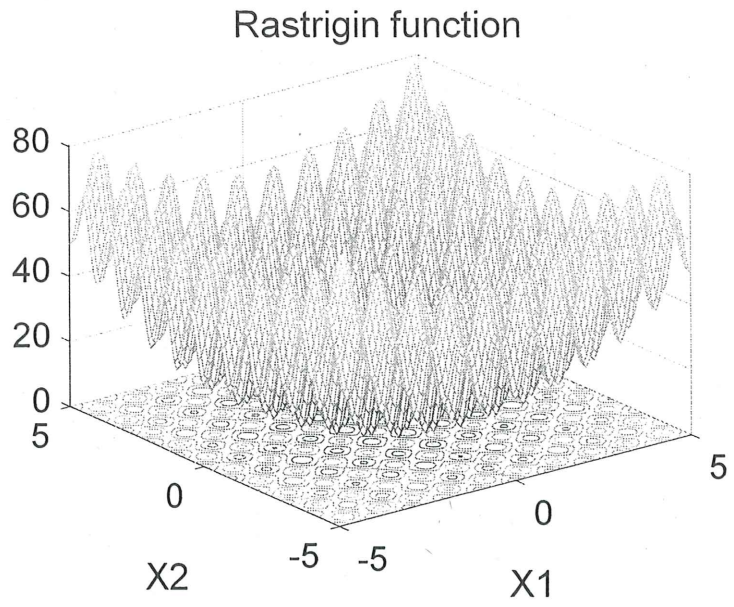

Fig. 2.2 Three-dimensional graph of function

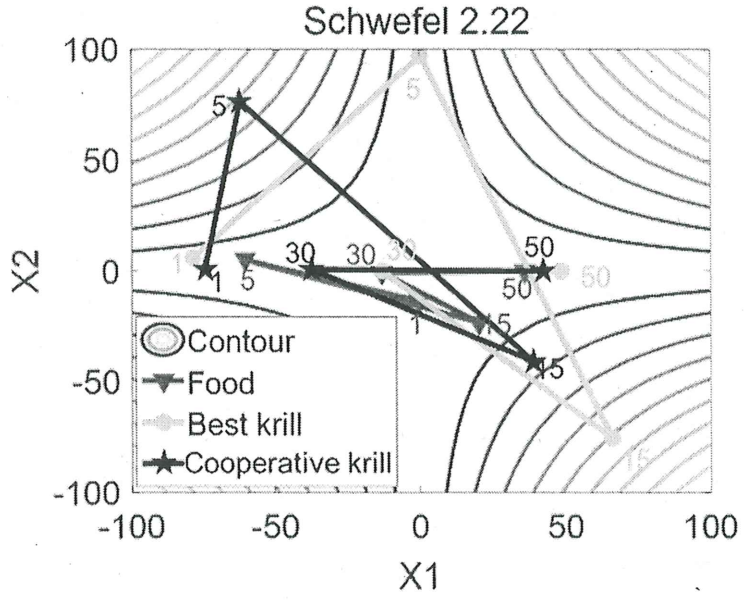

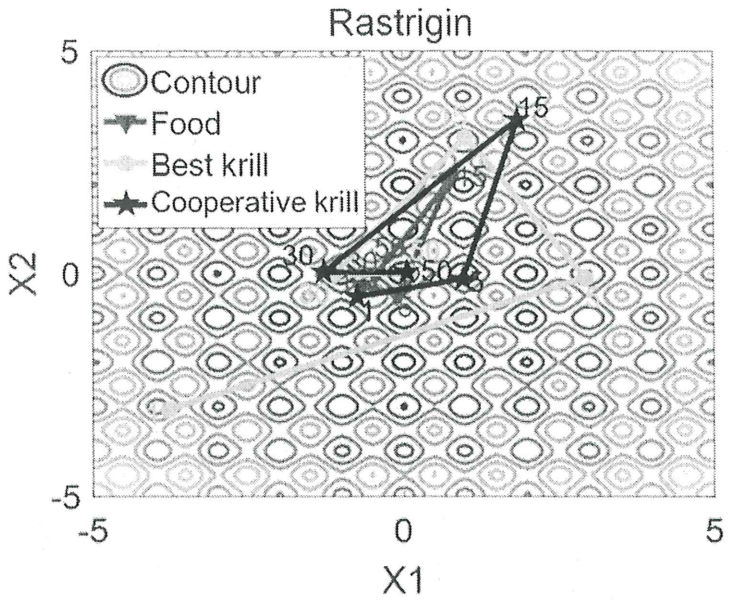

Fig. 2.3 Three particle optimization trajectories

After global exploration, the LMC operator was improved [40] to enhance the local exploitation. The LMC operator was inspired by the reproduction mechanism of GA; it prevented the premature fall into local optima by increasing the diversity of the population. However, the LMC operator only considered the "best krill" as the target for random crossover and mutation, which was not conducive to global optimization in the exploitation stage. The improved local mutation and crossover (ILMC) operator was developed to improve the local exploitation of TOKH. In ILMC operator, the optimum between the "center of food" and "best krill" served as the candidate solution, and the population learned from the candidate solution to accelerate aggregation to the optimum region in the exploitation stage. Algorithm 2 presents the pseudocode of ILMC operator.

In the Algorithm 2, X_{best} denotes the "best krill", X_{food} indicates the "center of food". d represents the decision variables. $X_i(j)$ denotes the j-th variable of the solution X_i. W_i indicates the offspring. j represents a random integer number between 1 and d obtained from a uniform distribution, and *rand* denotes a random real number in the interval (0, 1) obtained from a uniform distribution.

To make the ILMC mechanism easier to understand, an explanation is provided through the optimization of the krill swarm on the Sphere function. As shown in Fig. 2.4, in the process of krill population convergence, the "competitive krill" is closer to

the global optimum than worst krill and can carry out local exploitation in a better area to speed up the global convergence.

Algorithm 2：Pseudocode of the ILMC operator.

Begin

if X_{best} is better than X_{food}

$X_{cross} = X_{best}$

else

$X_{cross} = X_{food}$

end if

for $j = 1$ to d **do**

if $rand \leq 0.5$ **then**

$W_i(j) = X_{cross}(j)$

else $W_i(j) = X_{cross}(j)$

end if

end for j

Obtain the individual fitness value W_i

if W_i is better than X_i **then**

$X_i = W_i$

end

End

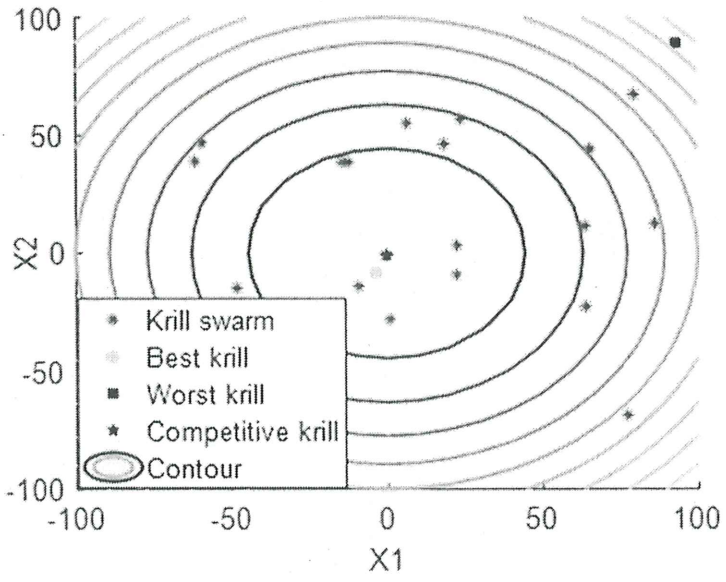

Fig. 2.4 Location distribution of the krill herd

Based on this analysis, the steps of the TOKH algorithm can be summarized as follows.

Step 1: Initialization: The generation counter was set to t=1, and the population P of NP krill individuals was randomly initialized. The foraging speed V_f, maximum diffusion speed D_{max}, and maximum induced speed N_{max} were also set.

Step 2: Krill population fitness evaluation: Each krill individual was evaluated according to its position.

Step 3: Motion calculation: The motion induced by the presence of other individuals was obtained using Eq. (2.2), the foraging motion was calculated using Eq. (2.4), and the physical diffusion was determined based on Eq. (2.6).

Step 4: The genetic operators [34] were implemented.

Step 5: Crossover operator: The "best krill" and "suboptimal krill" were crossed according to Algorithm 1.

Step 6: Population fine-tuning: The krill population was fine-tuned using ILMC operator in Algorithm 2. Each krill was evaluated considering its new position.

Step 7: Update the population position: The positions of krill individuals were updated in the search space.

Step 8: Repeat: steps 2–7 was repeated until a stop criterion was satisfied or a predefined number of iterations were completed.

Fig. 2.5 illustrates the flowchart of the TOKH algorithm.

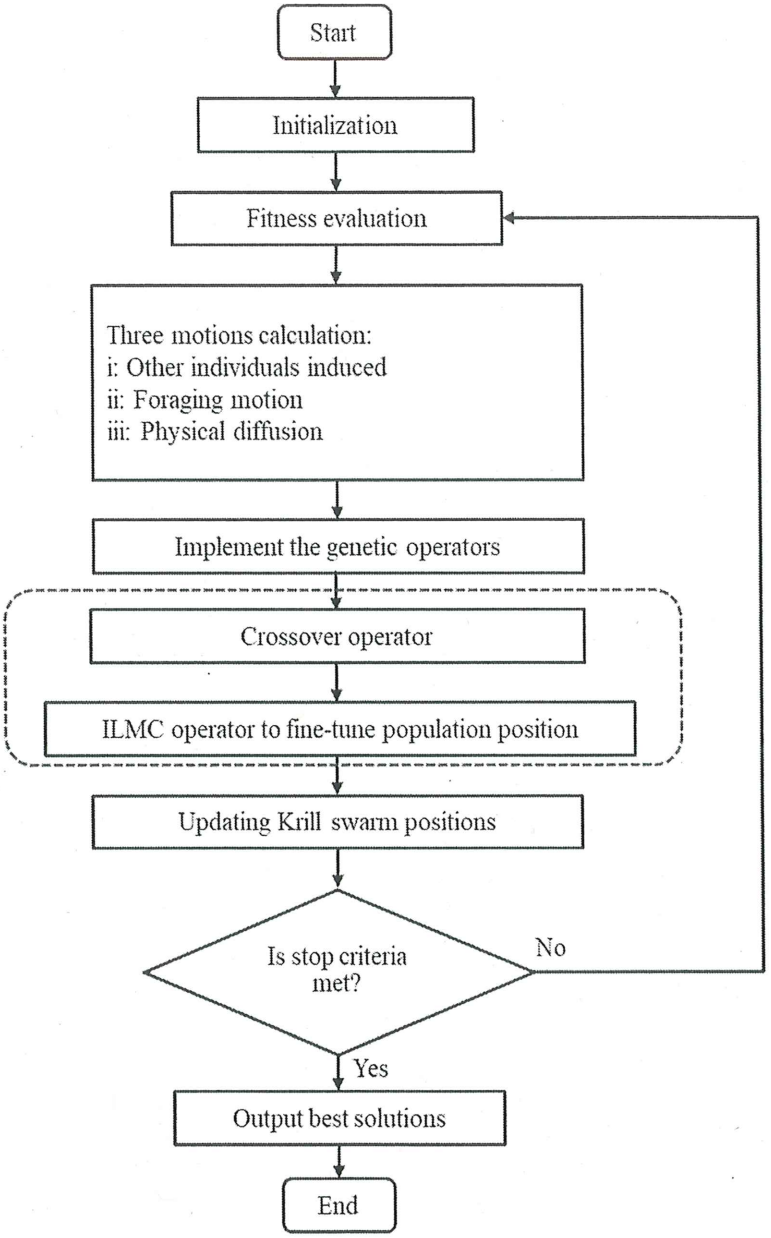

Fig. 2.5 TOKH algorithm flowchart

2.2 Time complexity analysis of TOKH

The time complexity of the algorithm was investigated to analyze the real-time efficiency of the TOKH algorithm in a better manner. The worst-case running time was expressed as a function of its input using a big Omicron (big-O) notation [48]. Typically, the big-O notation is used to denote an upper bound on the growth rate of a function and can be primarily applied to describe asymptotic behavior [48]. Logically, the big-O order is derived according to three rules:

1) All addition and subtraction constants during runtime are replaced by constant 1,

2) Only the highest order items are retained, and

3) The highest term constant is removed.

Firstly, TOKH algorithm is started with parameters initialization which requires constant time complexity $O(1)$. Secondly, in steps 2-4, three different movements of krill are implemented based on the rules of KH. The time complexity grows linearly according to the number of krill n, consequently, it requires $O(3n)$. Thirdly, referring to crossover operator and ILMC operator, the time complexity in step 5 and step 6 are equal to $O(1)$ and $O(n)$, respectively. Moreover, to implement the population update, the time complexity in step 7 is equal to $O(n)$. Finally in step 8, the population evolves according to a specific number of iterations t_{max}. Therefore, the total time complexity of TOKH is expressed by $O(1+(3n+1+n+n)\times t_{max}) \in O(n)$. In summary, it is obvious that most of the time complexity of TOKH comes from the basic KH, and the two operators introduced do not change the time complexity of TOKH.

The Rastrigin benchmark function [45] was selected for the verification. The functional dimensions were 30 and 100, and the population size was 50. All experiments were implemented and executed using MATLAB R2018a running on a personal computer with a 7-th generation core i7 CPU and Windows 10 OS. Fig. 2.6 depicts the experimental results for the time complexity.

As indicated in Fig. 2.6, the ordinate denotes the total time required in seconds for the algorithm to run 20 times on the Rastrigin benchmark function [45]. The abscissa represents the number of iterations, ranging from 0 to 1000; the running time was recorded once every 50 generations. The red and blue lines represent the fitting results of TOKH and KH algorithms, respectively. The running time and iteration of TOKH algorithm satisfied the linear relationship, and the time complexity of TOKH algorithm was $O(n)$. The experimental results validated that the two optimization operators introduced do not change the time complexity.

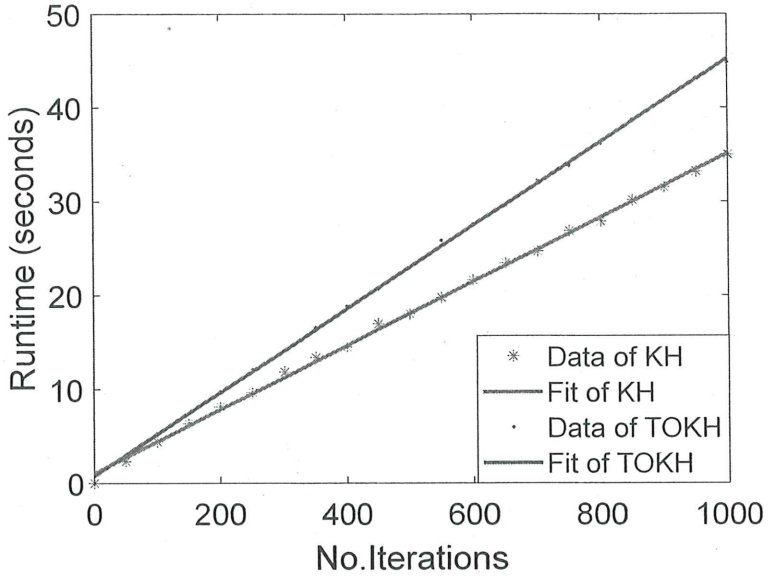

Fig. 2.6a 30 dimensions

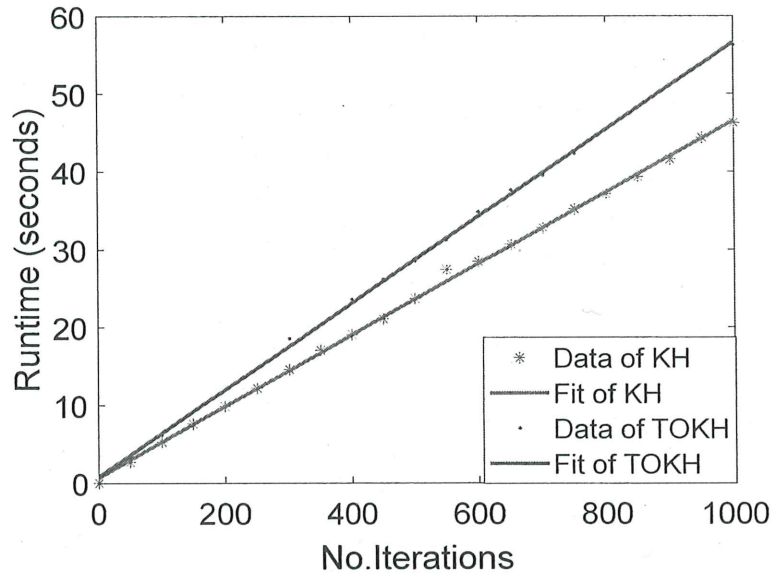

Fig. 2.6b 100 dimensions

Fig. 2.6 Relationship between the running time and number of iterations

2.3 Benchmark functions test

Fifteen benchmark functions were used to compare the optimized performance of TOKH algorithm with nine other versions of KH algorithm, including KH [34], CKH [38], OKH [39], MSKH [40], IKH [41], MKH [42], KHLD [43], SKH [44], and LKH [45]. Table 2.1 summarizes the specific parameter settings of each algorithm.

Benchmark functions are widely used for evaluating algorithm performance owing to their ease of implementation and high reliability. In this study, 15 different dimensional benchmark functions (Fig. 2.7) were selected to compare the performances of the algorithms. The dimensions (n) of the benchmark functions were set to 10, 30, and 50; the optimization performance of the 30-dimension was particularly analyzed, which is a pretty representation of the average performance of the algorithm. The expressions and properties of these benchmark functions have been reported in a previous study [38].

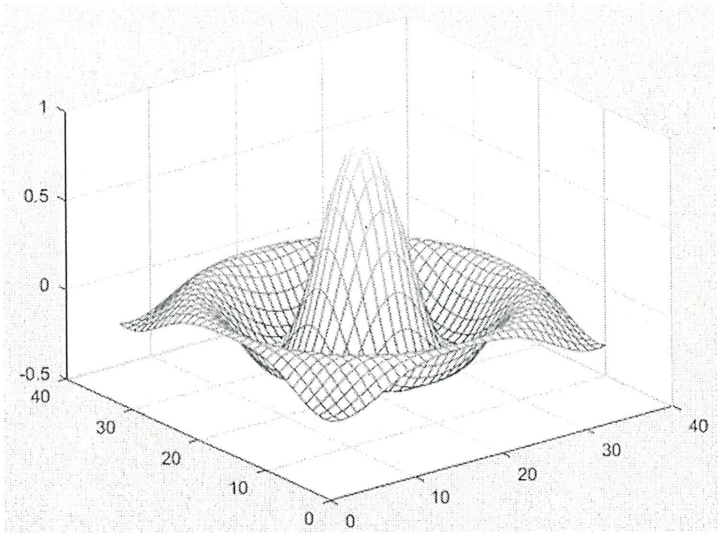

Unimodal function

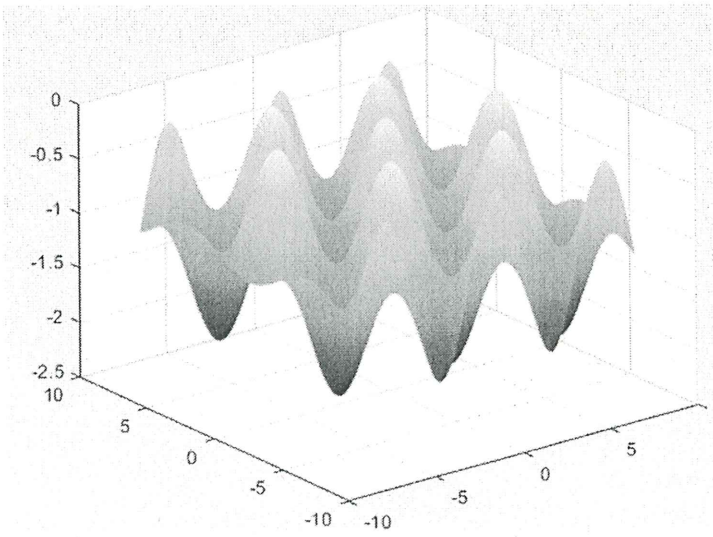

Multimodal function

Fig. 2.7 Benchmark functions

The population size *NP* of all algorithms was 50. The maximum number of iterations was 50, and 30 simulations were independently performed by each benchmark function. Tables 2.2–2.5 summarize the simulation results of the algorithm considering 30-dimension. Table 2.2 lists the best-optimized performances of these algorithms, whereas Table 2.3 presents the general optimization performance, Table 2.4 indicates the worst optimization performance, and Table 2.5 describes the stability. Tables 2.6 and 2.7 summarize the general optimization performance when the dimensions of the benchmark functions were 10 and 50, respectively.

When the dimension of the benchmark function was 30, TOKH and MSKH exhibited the best optimization performance for nine and seven benchmark functions, respectively (Table 2.2). TOKH algorithm performed better than the other KH algorithms on F1–F2, F6–F7, and F10–F14; MSKH algorithm performed best on F2–F5, F8–F9, and F15. About the general optimization performance (Table 2.3), TOKH algorithm performs best on ten benchmark functions (F1–F2, F4, F6–F7 and F10–F14) and MSKH algorithm performs best on five benchmark functions (F3, F5, F8–F9 and F15). Furthermore, TOKH algorithm performed best on twelve benchmark functions (F1–F2. F4, F6–F8 and F10–F15) with respect to the worst optimization performance (Table 2.4). In terms of stability (Table 2.5), TOKH algorithm exhibited the best stability for twelve benchmark functions (F1–F2. F4, F6–F8 and F10–F15). As indicated in Table 2.6, when the dimension of the benchmark function was 10, TOKH algorithm performed best on ten benchmark functions (F1–F4, F6–F7, F10–F12, and F14), MSKH algorithm performed best on F5 and F8–F9, and SKH exhibited the best performance on F15. When the dimension of the benchmark function was 50, TOKH algorithm performed best for all 15 benchmark functions (Table 2.7). Fig 2.8 illustrates the convergence process of several benchmark functions for 30-dimension. As indicated in the figure, TOKH algorithm was significantly superior to all other algorithms with respect to the optimization process.

Based on the data presented in Tables 2.2–2.7 and Fig 2.8, we concluded that the developed metaheuristic TOKH algorithm was more robust and stable than other metaheuristic search methods.

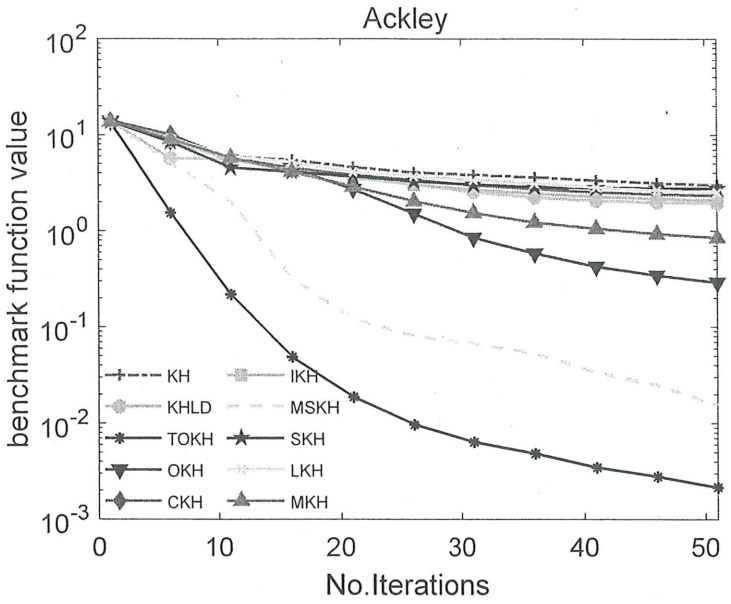
Ackley
benchmark function value
No.Iterations
KH
IKH
KHLD
MSKH
TOKH
SKH
OKH
LKH
CKH
MKH

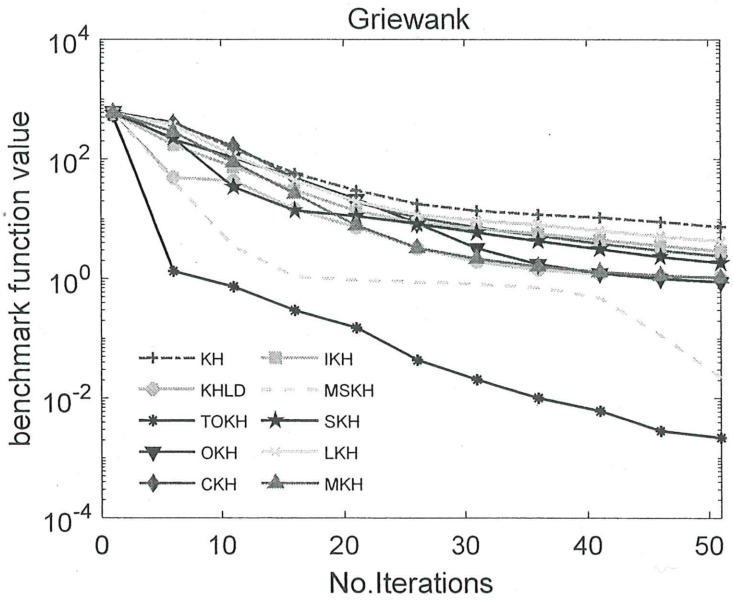
Griewank
benchmark function value
No.Iterations
KH
IKH
KHLD
MSKH
TOKH
SKH
OKH
LKH
CKH
MKH

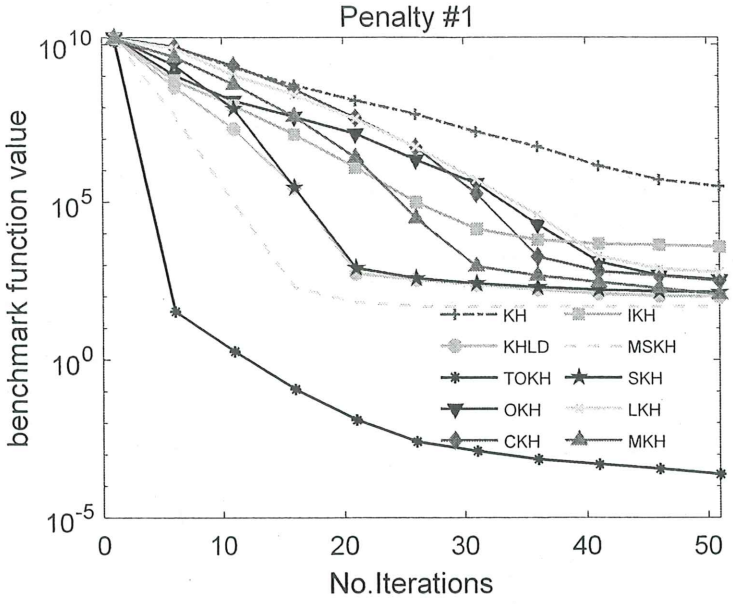
Penalty #1
benchmark function value
No.Iterations
KH
IKH
KHLD
MSKH
TOKH
SKH
OKH
LKH
CKH
MKH

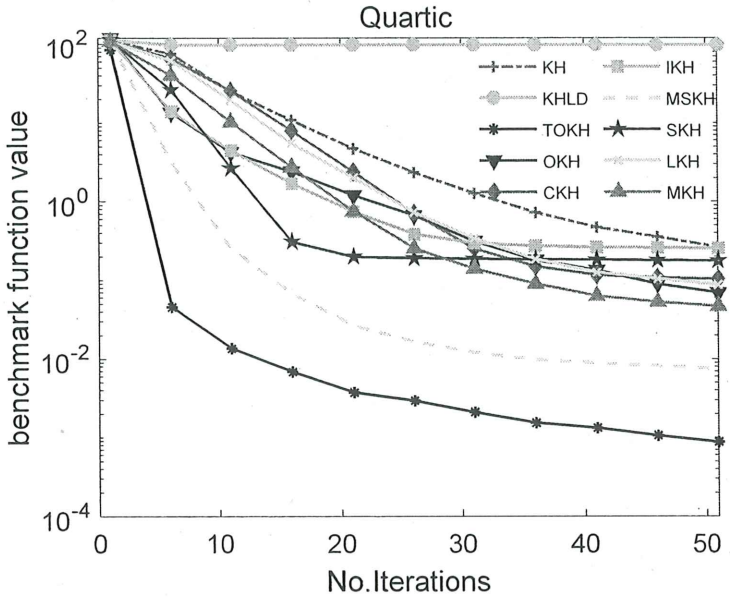
Quartic
benchmark function value
No.Iterations
KH
IKH
KHLD
MSKH
TOKH
SKH
OKH
LKH
CKH
MKH

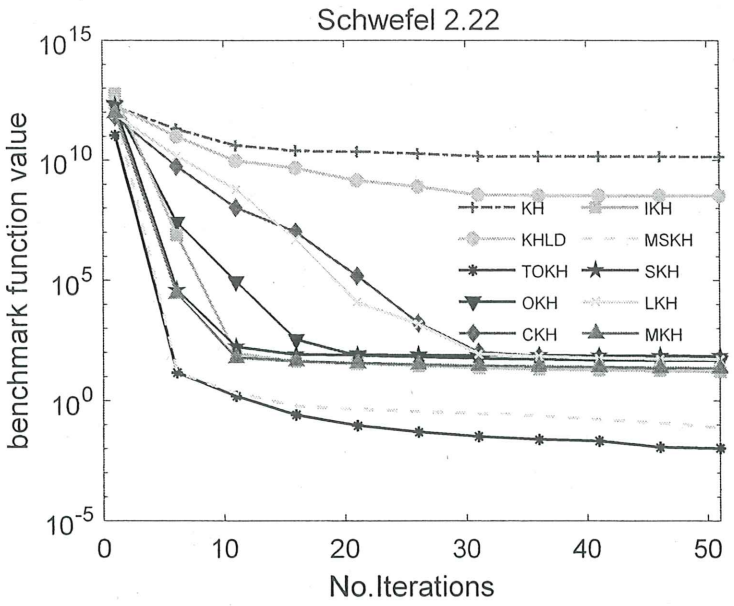
Schwefel 2.22
benchmark function value
No.Iterations
KH
IKH
KHLD
MSKH
TOKH
SKH
OKH
LKH
CKH
MKH

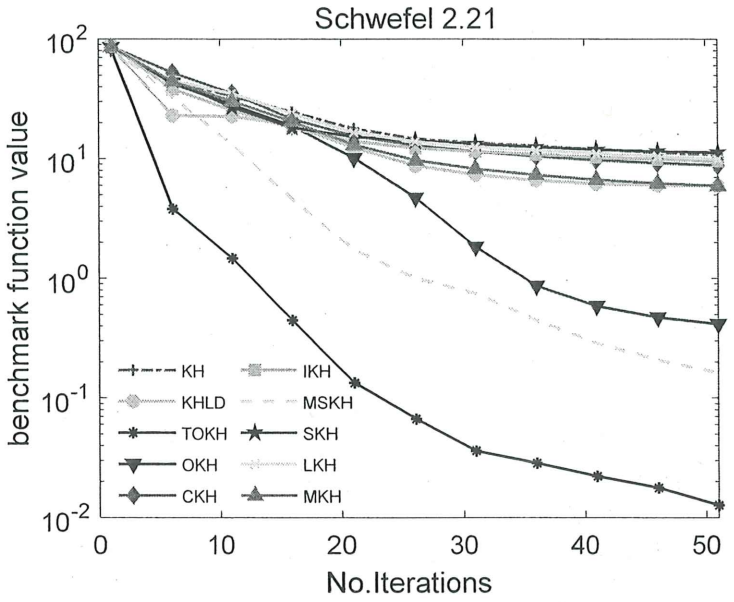
Schwefel 2.21
benchmark function value
No.Iterations
KH
IKH
KHLD
MSKH
TOKH
SKH
OKH
LKH
CKH
MKH

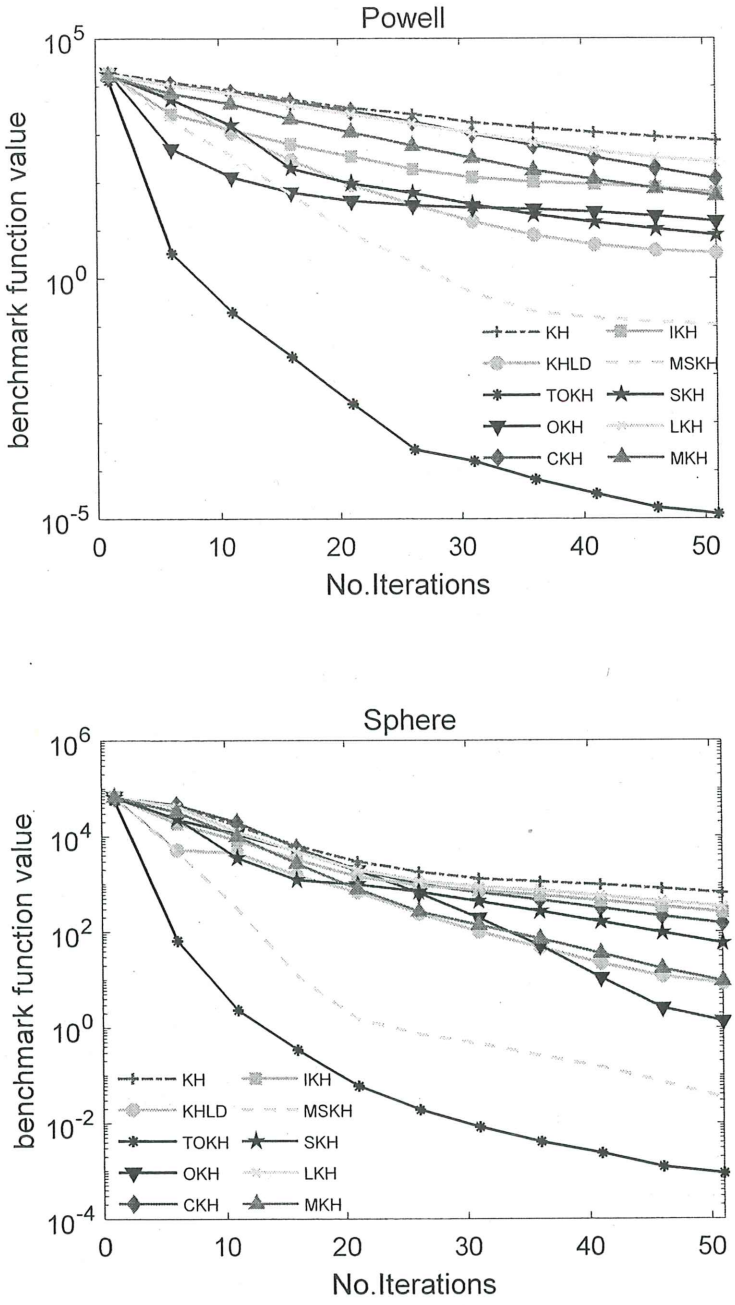

Fig 2.8 Performance comparison considering the 30-dimension benchmark functions

Table 2.1
Specific parameter settings of each algorithm.

Algorithm name	Basic parameters
KH	The maximum induced speed $N^{max} = 0.01$, the foraging speed $V_f = 0.02$, the maximum diffusion speed $D^{max} = 0.005$.
KHLD	$Ct_{max} = 2$, $Ct_{min} = 0$, Other parameters are the same as KH.
TOKH	All parameters are the same as KH.
OKH	Reference [39], OKH7 is selected. δ_1=0.4, δ_2 =0.6. Other parameters are the same as KH.
CKH	Reference [38], M10 chaotic map is selected. Other parameters are the same as KH.
IKH	Reference [41], IKH2 is selected. Other parameters are the same as KH.
MSKH	All parameters are the same as KH.
SKH	Reference [44], SKH1 is selected. Crossover probability of single point crossover Pc=1. Other parameters are the same as KH.
LKH	Max Levy-flight step size $A = 1.0$. Other parameters are the same as KH.
MKH	Elitism parameter $Keep = 2$, Other parameters are the same as KH.

Table 2.2

Best values of the benchmark functions (the dimension of function is 30).

	KH	KHLD	TOKH	OKH	CKH	IKH	MSKH	SKH	LKH	MKH
F1	1.95	0.29	**0.00**	0.040	1.60	1.57	0.012	1.36	1.84	0.051
F2	2.67	0.99	**0.00**	0.61	1.23	1.62	**0.00**	1.05	2.20	0.89
F3	6.71E1	1.01E1	4.58E-3	8.38E-1	2.15E1	1.33E1	**7.59E-4**	1.78E1	2.37E1	3.09
F4	1.47E3	3.67E1	4.26E-5	9.34E1	1.33E2	1.34E2	**1.10E-5**	5.06E1	2.17E2	3.33E1
F5	4.52E3	7.82	2.32E-5	1.67	1.89E1	2.82E1	**8.57E-6**	1.64E1	2.21E1	3.11
F6	8.04E-2	5.82E-2	**1.80E-4**	1.06E-2	3.38E-2	7.05E-2	6.84E-4	5.04E-2	3.74E-2	1.22E-2
F7	1.60E2	6.85	**8.63E-7**	8.88E1	9.24E1	4.64E1	5.37E-3	6.24E1	8.88E1	5.05E1
F8	5.25E1	2.79E1	2.71E1	1.13E1	3.33E1	3.61E1	**2.48E-3**	2.86E1	3.82E1	2.95E1
F9	8.66E3	8.23E3	1.21E-1	2.20E3	6.04E3	2.20E3	**2.21E-2**	2.84E3	5.20E3	1.25E3
F10	2.35E4	4.30	**1.86E-5**	7.46E3	1.44E4	2.89E3	1.26	6.19E2	1.80E4	8.67E3
F11	1.26E4	9.45E3	**1.80E-3**	1.88E1	3.62E1	8.65	3.14E-2	3.57E1	3.39E1	7.92
F12	6.94	2.26	**8.94E-4**	2.78E-1	6.00	6.53	3.57E-2	7.36	5.28	3.81
F13	3.26E2	2.24	**2.03E-5**	5.03E-1	5.04E1	8.42E1	1.49E-2	3.46	6.73E1	1.31
F14	4.41E2	4.84E-1	**4.70E-8**	1.48E-1	3.51E1	1.43E1	1.50E-4	1.06	1.04E2	8.65
F15	4.72E2	3.98	6.67E-1	1.35	3.99E1	6.43E1	**9.73E-2**	4.34	1.09E2	3.37
Sun	0	0	9	0	0	0	7	0	0	0

Table 2.3

Mean values of the benchmark functions (the dimension of function is 30).

	KH	KHLD	TOKH	OKH	CKH	IKH	MSKH	SKH	LKH	MKH
F1	2.74	1.79	**0.00**	0.34	2.30	2.13	0.022	2.65	2.67	0.72
F2	6.25	1.11	**0.00**	0.88	2.65	3.51	0.020	1.66	3.79	1.08
F3	1.50E2	2.64E1	9.88E-3	1.37E1	5.28E1	3.29E1	**3.11E-3**	6.71E1	7.99E1	7.34
F4	3.02E5	1.30E2	**2.30E-4**	3.84E2	3.36E2	1.47E3	1.56E1	1.49E2	5.70E2	1.09E2
F5	1.50E5	2.47E1	1.58E-4	4.01E2	8.76E1	1.73E3	**3.93E-5**	3.63E1	1.50E3	9.94
F6	3.59E-1	9.25E1	**8.26E-4**	6.78E-2	1.11E-1	2.09E-1	4.04E-3	1.84E-1	9.38E-2	4.08E-2
F7	2.03E2	5.39E1	**3.99E-4**	1.58E2	1.49E2	8.04E1	3.00	1.24E2	1.30E2	7.12E1
F8	8.82E1	2.92E1	2.74E1	3.07E1	4.65E1	6.04E1	**2.69E1**	3.34E1	6.14E1	3.76E1
F9	9.35E3	9.48E3	2.80E-1	3.51E3	6.82E3	3.86E3	**1.18E-1**	4.37E3	6.41E3	2.24E3
F10	3.86E4	7.85E3	**8.53E-4**	1.71E4	2.41E4	7.43E3	2.10E3	3.54E3	2.83E4	1.32E4
F11	9.55E9	3.62E9	**1.12E-2**	3.96E1	4.91E1	1.76E1	7.09E-2	6.98E1	4.82E1	2.42E1
F12	1.01E1	5.80	**1.38E-2**	3.98E-1	8.82	1.01E1	2.83E-1	1.24E1	1.01E1	6.66
F13	6.52E2	9.66	**8.86E-4**	1.74	1.62E2	3.43E2	3.56E-2	5.71E1	3.17E2	9.67
F14	8.70E2	3.25	**1.16E-5**	1.88E1	1.10E2	7.11E1	1.50E-1	1.07E1	3.05E2	5.62E1
F15	2.27E3	8.99	6.67E-1	1.63E2	1.77E2	3.73E2	**4.63E-1**	1.70E1	4.56E2	1.83E1
Sun	0	0	10	0	0	0	5	0	0	0

Table 2.4

Worst values of the benchmark functions (the dimension of function is 30).

	KH	KHLD	TOKH	OKH	CKH	IKH	MSKH	SKH	LKH	MKH
F1	3.39	2.76	**0.010**	1.19	3.45	2.86	0.031	3.36	3.34	1.65
F2	16.09	1.68	**0.010**	1.23	4.65	6.00	0.063	2.94	6.55	1.24
F3	2.40E2	5.93E1	1.67E-2	8.43E1	1.49E2	7.51E1	**6.55E-3**	2.59E2	1.74E2	1.89E1
F4	1.91E6	3.31E2	**6.85E-4**	9.33E2	5.06E2	2.54E4	9.35E1	5.63E2	1.07E3	2.95E2
F5	7.95E5	4.91E1	5.12E-4	7.30E3	9.46E2	1.31E4	**9.79E-5**	5.19E1	7.13E3	2.33E1
F6	7.97E-1	1.50E2	**2.77E-3**	1.74E-1	1.80E-1	6.17E-1	1.79E-2	4.28E-1	2.77E-1	7.70E-2
F7	2.32E2	1.86E2	**1.58E-3**	2.04E2	1.84E2	1.25E2	2.99E1	2.58E2	1.61E2	1.07E2
F8	1.40E2	3.30E1	**2.77E1**	5.23E1	6.40E1	8.74E1	2.81E1	4.78E1	1.11E2	5.06E1
F9	1.01E4	1.01E4	3.82E-1	5.61E3	8.58E3	4.91E3	**2.67E-1**	5.46E3	7.19E3	3.30E3
F10	6.09E4	1.43E4	**5.16E-3**	2.73E4	3.58E4	1.28E4	1.50E4	1.23E4	3.59E4	1.87E4
F11	1.28E11	8.28E10	**2.53E-2**	6.32E1	7.61E1	3.32E1	1.04E-1	1.02E2	6.62E1	5.85E1
F12	1.39E1	9.94	**4.85E-2**	7.74E-1	1.34E1	1.71E1	3.48	1.99E1	1.36E1	1.11E1
F13	1.44E3	3.33E1	**3.56E-3**	8.94	4.38E2	7.61E2	9.15E-2	2.97E2	5.89E2	3.67E1
F14	1.42E3	1.05E1	**8.07E-5**	7.34E1	2.48E2	1.66E2	2.98	7.77E1	5.74E2	1.52E2
F15	7.37E3	1.74E1	**6.67E-1**	2.74E3	6.38E2	1.19E3	7.51E-1	4.85E1	1.07E3	4.35E1
Sun	0	0	12	0	0	0	3	0	0	0

Table 2.5

Standard deviations of the benchmark functions (the dimension of function is 30).

	KH	KHLD	TOKH	OKH	CKH	IKH	MSKH	SKH	LKH	MKH
F1	0.34	0.49	**0.00**	0.37	0.46	0.34	0.00	0.48	0.35	0.56
F2	2.72	0.14	**0.00**	0.14	0.96	1.20	0.010	0.54	1.26	0.080
F3	5.00E1	1.20E1	3.27E-3	2.02E1	2.87E1	1.36E1	**1.67E-3**	5.90E1	2.86E1	3.75
F4	4.58E5	7.71E1	**1.31E-4**	1.88E2	9.86E1	4.78E3	3.54E1	1.02E2	2.15E2	6.24E1
F5	1.85E5	7.91	9.96E-5	1.41E3	1.73E2	2.99E3	**2.35E-5**	8.19	2.22E3	5.55
F6	2.07E-1	3.05E1	**5.88E-4**	4.06E-2	4.66E-2	1.30E-1	4.07E-3	9.48E-2	4.72E-2	2.04E-2
F7	1.85E1	5.57E1	**4.17E-4**	2.50E1	2.12E1	1.90E1	9.11	4.77E1	2.00E1	1.34E1
F8	2.27E1	1.01	**1.39E-1**	5.71	8.83	1.48E1	5.08	4.51	1.55E1	5.61
F9	3.67E2	4.13E2	7.16E-2	5.18E2	5.58E2	7.37E2	**5.56E-2**	6.88E2	5.09E2	4.59E2
F10	9.81E3	2.67E3	**1.30E-3**	4.66E3	5.62E3	2.21E3	3.43E3	2.67E3	4.69E3	3.08E3
F11	2.58E10	1.52E10	**6.17E-3**	1.12E1	7.96	5.88	1.55E-2	1.80E1	9.94	1.10E1
F12	1.93	1.84	**1.00E-2**	1.13E-1	1.57	2.39	6.51E-1	3.57	2.13	1.57
F13	2.69E2	7.66	**9.11E-4**	1.57	9.20E1	1.86E2	1.81E-2	6.51E1	1.52E2	7.71
F14	2.71E2	2.56	**1.65E-5**	1.82E1	4.93E1	4.20E1	5.52E-1	1.58E1	1.13E2	3.81E1
F15	1.79E3	3.61	**5.61E-5**	5.05E2	1.34E2	2.77E2	2.32E-1	1.00E1	2.73E2	9.04
Sun	0	0	12	0	0	0	3	0	0	0

Table 2.6

Mean values of the benchmark functions (the dimension of function is 10).

	KH	KHLD	TOKH	OKH	CKH	IKH	MSKH	SKH	LKH	MKH
F1	2.11	2.00E-2	**0.00**	1.20E-1	5.40E-1	4.10E-1	4.50E-2	1.37	1.42	6.10E-2
F2	6.20E-1	1.40E-1	**0.00**	5.30E-1	5.00E-1	2.20E-1	3.40E-2	2.70E-1	4.10E-1	2.60E-1
F3	9.68	9.00E-2	**0.00**	3.50E-1	3.42	2.06	9.40E-1	2.15E1	3.15	9.10E-2
F4	2.56E1	1.56	**1.63E-4**	4.30E-1	4.48	2.09	3.46	1.19E1	5.39	3.10E-1
F5	7.06	9.00E-2	1.44E-4	2.00E-1	5.00E-1	5.90E-1	**5.43E-6**	1.24	2.01	1.33E-4
F6	7.00E-3	1.70E-3	**1.00E-4**	3.79E-4	8.41E-4	5.18E-4	2.00E-2	2.40E-3	1.20E-3	3.14E-4
F7	5.30E-2	9.90E-1	**1.03E-5**	9.80E-2	1.18	2.98	1.00E-3	4.97	2.05	1.20E-1
F8	8.12	5.77	6.56	1.42	5.66	1.30E-1	**9.08E-5**	4.40	5.46	2.01
F9	1.99E3	1.65E3	1.50E-2	8.55E2	6.74E2	4.60E-2	**1.60E-3**	3.36E2	7.38E2	1.50E-2
F10	4.47E2	1.72E1	**8.77E-6**	2.35E1	1.67E2	6.11	6.99E-5	3.80E-1	1.27E2	6.10E-1
F11	1.81E1	6.27	**5.18E-4**	1.94	5.00E-1	2.90E-3	1.82E-3	1.85E-3	4.96	4.56E-3
F12	4.40E-2	1.70E-2	**1.70E-3**	5.90E-2	5.30E-2	7.00E-3	1.10E-2	5.00E-3	1.80E-2	6.90E-3
F13	1.10E-2	2.50E-3	3.14E-5	8.20E-3	7.90E-3	**5.33E-6**	1.50E-3	3.05E-6	3.85E-4	2.77E-5
F14	6.45	2.20E-3	**1.37E-9**	8.08E-4	2.00E-2	2.29E-4	4.04E-7	1.87E-4	5.60E-1	2.55E-5
F15	7.10E-1	6.60E-1	4.08E-4	6.70E-1	1.00E-1	1.00E-1	1.01E-4	**7.41E-5**	1.30E-1	2.20E-3
Sun	0	0	10	0	0	1	3	1	0	0

Table 2.7

Mean values of the benchmark functions (the dimension of function is 50).

	KH	KHLD	TOKH	OKH	CKH	IKH	MSKH	SKH	LKH	MKH
F1	1.11E1	7.45	**8.60E-3**	3.83	1.05E1	1.02E1	8.03E-2	1.07E1	1.06E1	8.48
F2	4.41E1	2.05E1	**1.90E-3**	1.03	3.43E1	4.52E1	9.29E-2	2.99E1	3.50E1	1.87E1
F3	4.91E1	8.99	**1.30E-3**	3.33	2.45E1	2.86E1	7.11E-2	2.16E1	2.52E1	9.93
F4	8.02E6	2.86E3	**4.60E-3**	3.28E2	1.98E6	7.56E6	6.78E1	6.37E3	2.88E6	2.51E5
F5	2.07E6	1.70E4	**2.20E-3**	5.14	8.07E5	1.54E6	1.57	1.13E5	6.99E5	2.05E5
F6	2.51	4.09E2	**3.00E-3**	5.80E-2	1.52	2.01	2.84E-2	1.78	1.59	8.52E-1
F7	4.48E2	2.17E2	**2.00E-3**	3.03E2	3.37E2	2.61E2	1.40E1	3.22E2	2.75E2	2.04E2
F8	1.95E6	2.45E5	**4.88E1**	7.64E2	1.21E6	1.66E6	6.79E1	5.10E5	1.11E6	4.13E5
F9	1.75E4	1.73E4	**9.00E-1**	7.40E3	1.39E4	1.05E4	1.19E2	1.07E4	1.36E4	8.23E3
F10	1.56E5	3.53E4	**2.31**	4.12E4	7.81E4	4.98E4	5.17E4	3.55E4	2.17E4	5.88E4
F11	4.20E22	2.76E20	**2.46E-2**	1.50E9	1.07E10	8.99E1	1.71E-1	1.71E2	9.83E7	1.26E2
F12	2.48E1	1.42E1	**2.10E-2**	3.32E-1	2.29E1	2.44E1	1.16	2.54E1	2.02E1	2.11E1
F13	4.78E3	2.03E3	**1.70E-3**	1.45E1	4.19E3	4.72E3	1.13E-1	3.14E3	4.44E3	1.87E3
F14	3.27E3	1.14E2	**6.29E-5**	4.42E1	6.15E2	7.68E2	2.45E1	2.14E2	5.27E2	3.35E2
F15	3.02E4	3.02E3	**8.42E-1**	6.05	1.57E4	2.08E4	2.54	7.15E3	1.60E4	6.28E3
Sun	0	0	15	0	0	0	0	0	0	0

2.4 Truss optimization

To further investigate the robustness of TOKH algorithm for truss optimization, we solved the weight minimization problems of four truss structures under multiple loading conditions using discrete variables. The algorithms were coded in MATLAB and the structures were analyzed using the direct stiffness method. The optimization results were compared to the results obtained from other optimization methods (including TLBO [23], PO [28], MRFO [33], KH [34], CKH [38], OKH [39], IKH [41], KHLD [43], and LKH [45].) in the literature to evaluate the robustness of TOKH algorithm. Twenty independent runs were performed for each design problem with the population size of each algorithm set to 30.

2.4.1 Computational model

Discrete sizing optimization of the truss attempts to identify the optimal cross-section of the system elements to minimize the structural weight. Moreover, the minimum design must satisfy the inequality constraints that limit the design variable sizes and structural responses [46].

The discrete structural optimization problem for a truss can be formulated as [28]:

$$\begin{aligned} &\text{Find} && S=[S_1,S_2,...,S_v],\\ &&& S_i \in D_i, D_i=[d_{i,1},d_{i,2},...,d_{i,r(i)}]\\ &\text{To minimize} && W(S)=\sum_{i=1}^{nm}\gamma_i \bullet S_i \bullet L_i \\ &\text{Subject to} && \sigma_{\min} \le \sigma_i \le \sigma_{\max} \quad i=1,2,...,n\\ &&& \delta_{\min} \le \delta_j \le \delta_{\max} \quad j=1,2,...,m \end{aligned} \tag{2.9}$$

Here, S represents the set of design variables, D_i denotes an allowable set of discrete values for design variable S_i, v indicates the number of design variables or member groups, $r(i)$ represents the number of available discrete values for the i-th design variable, $W(S)$ denotes the weight of the structure, n indicates the number of component members in the structure, m represents the number of nodes, γ_i denotes the material density of member I, L_i indicates the length of member i, δ_j represents the nodal displacement/deflection at node j, σ_i denotes the stress developed in the i-th element, and $\delta_{\min}$ and $\delta_{\max}$ represent the lower and upper bounds, respectively.

The optimum design of truss structures must satisfy the optimization constraints stated in Eq. (1). This procedure comprises the following three rules:

Rule 1: Any feasible solution is better than any infeasible solution.

Rule 2: Between two feasible solutions, a solution with a better objective function value is preferable.

Rule 3: Between two infeasible solutions, the solution with the smallest constraint violation is preferred.

The first and third rules direct the search toward feasible regions, whereas the second rule directs the search to a feasible region with suitable solutions [47].

2.4.2 Planar 10-bar truss

The planar 10-bar truss structure is one of the most popular test problems in structural optimization, previously solved in [49]. Fig 2.9 depicts the geometry and support conditions followed for this two-dimensional, cantilevered truss under loading conditions. As indicated in the figure a static load of 100 kips was applied downward to two nodes. To satisfy the stress and displacement constraints, the minimum weight of the 10-bar truss was obtained by adjusting the cross-sectional area of each member. A set of 41 discrete values were used for the possible cross-sectional areas for each member, as follows: S ={1.62, 1.80, 1.99, 2.13, 2.38, 2.62, 2.88, 2.93, 3.09, 3.13, 3.38, 3.47, 3.55, 3.63, 3.84, 3.87, 3.88, 4.18, 4.22, 4.49, 4.59,4.80, 4.97, 5.12, 5.74, 7.22, 7.97, 11.5, 13.5, 13.9, 14.2, 15.5, 16.0, 16.9, 18.8, 19.9, 22.0, 22.9, 26.5, 30.0, 33.5} (in^2). The combined size of all feasible solutions was $(41)^{10}$. The Young's modulus of the material was 10^7 psi, and the weight density was 0.1 lb/in^3. The displacement constraints in the X and Y directions at each node were limited to 2 in. The restraining stress of each member was less than 25 ksi.

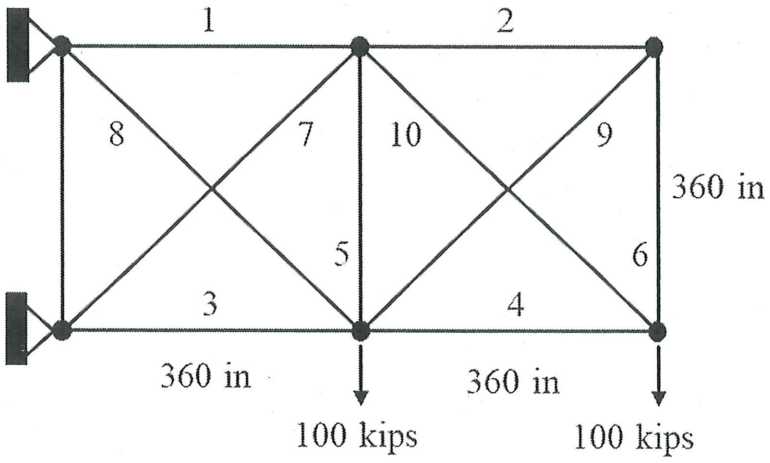

Fig 2.9 10-bar truss

Table 2.8 summarizes the optimal designs and their corresponding number of structural analyses (NSA) using the TOKH with nine other methods. TOKH, TLBO, and MRFO achieved the lightest designs. However, statistical results after 20 runs also demonstrate that TLBO and MRFO exhibited less stability compared to TOKH. Based on the average of 20 independent runs, the NSA is 3100 for TOKH and 1580 required for KH. Although TOKH has 1520 more structural analyses than KH, the optimization efficiency of TOKH algorithm is 20.90% higher than that of KH algorithm. Fig 2.10 shows the average convergence curves obtained for TOKH and the nine different methods when the planar 10-bar truss is applied. This is a relatively simple structural sizing optimization problem, and its optimal sizing is easy to find. It is obvious that through efficient global exploration, TOKH quickly converges to the minimum with fewer iterations. The TOKH algorithm has the highest global convergence rate. For other algorithms, MRFO works very well, because it ranks 2 among ten methods.

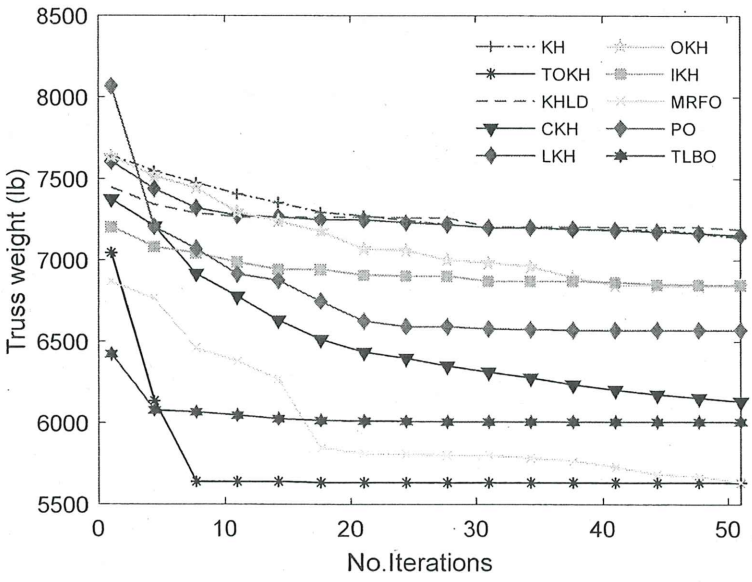

Fig 2.10 Algorithm optimization process of the 10-bar truss

Table 2.8
Optimized designs for the 10-bar truss.

	KH	KHLD	CKH	LKH	IKH	TOKH	OKH	TLBO	PO	MRFO
S_1	30.00	33.50	33.50	30.00	30.00	33.50	28.50	33.50	33.50	33.50
S_2	1.62	3.55	5.94	2.13	1.80	1.62	13.50	1.62	1.62	1.62
S_3	28.50	28.50	22.90	28.50	22.90	22.90	30.00	22.90	22.90	22.90
S_4	15.50	11.50	15.50	11.50	18.80	14.20	18.80	14.20	15.50	14.20
S_5	1.62	1.62	1.62	1.62	1.62	1.62	5.94	1.62	1.62	1.62
S_6	1.62	5.94	1.62	1.99	1.62	1.62	5.94	1.62	1.62	1.62
S_7	19.90	18.80	22.00	16.90	22.90	22.90	22.90	22.90	18.80	22.90
S_8	7.97	11.50	7.97	16.00	11.50	7.97	7.22	7.97	7.22	7.97
S_9	2.13	3.55	1.62	4.18	1.62	1.62	5.94	1.62	1.62	1.62
S_{10}	22.00	18.80	22.00	22.90	18.80	22.90	18.80	22.90	28.50	22.90
NSA	1580.00	1580.00	1580.00	3080.00	1930.00	3100.00	6080.00	4410.00	1780.00	3030.00
Computational time (s)	1.33	1.42	1.51	1.81	1.64	1.80	3.01	1.54	0.50	0.58
Optimal value (lb)	5.63E3	5.83E3	5.65E3	5.78E3	5.59E3	**5.49E3**	6.54E3	**5.49E3**	5.62E3	**5.49E3**
Mean (lb)	7.13E3	7.19E3	6.13E3	7.15E3	6.85E3	**5.64E3**	6.83E3	5.91E3	6.56E3	5.66E3
Std (lb)	1.51E3	9.66E2	2.53E2	1.31E3	1.14E3	**4.84E1**	2.86E2	2.50E2	8.01E2	1.09E2
Increased efficiency	~	-0.84%	14.03%	-0.28%	3.93%	**20.90%**	4.21%	17.11%	7.99%	20.62%

2.4.3 Spatial 25-bar truss

Fig 2.11 illustrates the 25-bar transmission tower spatial truss, which has been analyzed by several researchers [49]. All structural elements were organized into eight groups, where the members of each group shared the same material and cross-sectional properties. Table 2.9 presents each element group according to the member number; (each member is defined based on its start and end node numbers). Table 2.10 lists the coordinates of the 25-bar truss nodes. The Young's modulus of the material was 10^7 psi, and the weight density was 0.1 lb/in^3. A single load case was applied to the structure in the design of the 25-bar truss (Table 11). The allowable stresses for each member were ±40 ksi and the allowable displacements for each node in the X, Y and Z directions were ±0.35 in. Discrete values for each cross-sectional area were obtained from the available set S = {0.1, 0.2, 0.3, 0.4, 0.5, 0.6, 0.7, 0.8, 0.9, 1.0, 1.1, 1.2, 1.3, 1.4, 1.5, 1.6, 1.7, 1.8, 1.9, 2.0, 2.1, 2.2, 2.3, 2.4, 2.5, 2.6, 2.7, 2.8, 2.9, 3.0, 3.1, 3.2, 3.3, 3.4} (in^2). The size of the design search space was $(34)^8$.

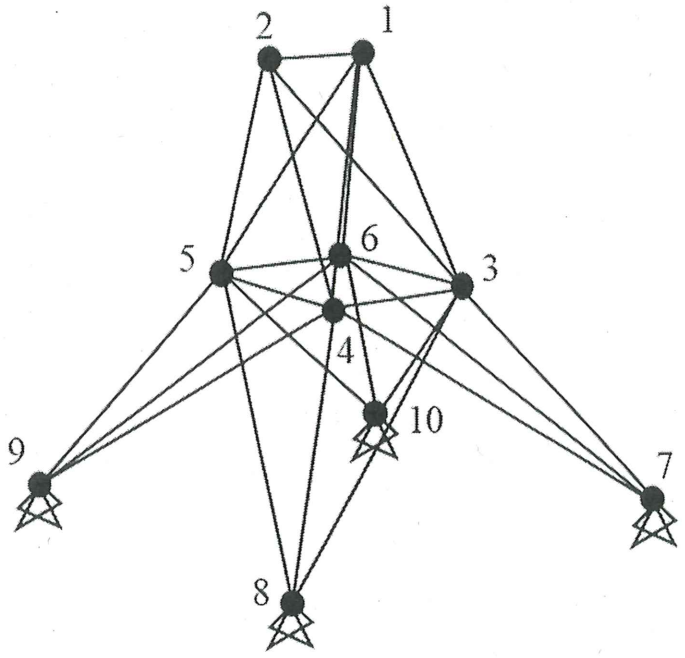

Fig 2.11 25-bar truss

Table 2.12 compares the final optimum design and the corresponding results calculated by the ten methods. Compared with the other nine methods, TOKH algorithm still has the robustness. The average weight gained by TOKH algorithm is 488.34 lb, 17.37% lighter than that of KH algorithm. The standard deviation with the TOKH algorithm is 2.59, which is the

lowest among all methods. Fig 2.12 depicts the average convergence curves for the 25-bar truss. TOKH quickly converges to a better global region in the early iterations and continues to search the minimum in about 10-20 iterations through local exploitation. MRFO algorithm converges slowly in the early stage and gradually overtakes TLBO and PO in the late iteration.

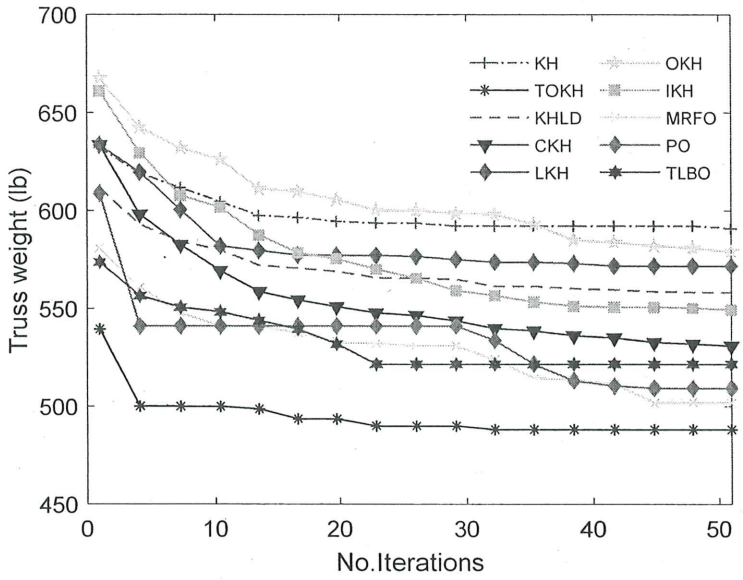

Fig 2.12 Algorithm optimization process of the 25-bar truss

Table 2.9

Element information for the 25-bar truss.

Design variables	Members
S1	(1,2)
S2	(1,4), (2,3), (1,5), (2,6)
S3	(2,5), (2,4), (1,3), (1,6)
S4	(3,6), (4,5)
S5	(3,4), (5,6)
S6	(3,10), (6,7), (4,9), (5,8)
S7	(3,8), (4,7), (6,9), (5,10)
S8	(3,7), (4,8), (5,9), (6,10)

Table 2.10

Nodal coordinates for the 25-bar truss.

Node	X (in.)	Y (in.)	Z (in.)
1	-37.5	0.0	200.0
2	37.5	0.0	200.0
3	-37.5	37.5	100.0
4	37.5	37.5	100.0
5	37.5	-37.5	100.0
6	-37.5	-37.5	100.0
7	-100.0	100.0	0.0
8	100.0	100.0	0.0
9	100.0	-100.0	0.0
10	-100.0	-100.0	0.0

Table 2.11
Loading conditions for the 25-bar truss.

Node	P_x (kips)	P_y (kips)	P_z (kips)
1	1.0	-10.0	-10.0
2	0.0	-10.0	-10.0
3	0.5	0.0	0.0
6	0.6	0.0	0.0

Table 12
Optimized designs for the 25-bar truss.

	KH	KHLD	CKH	LKH	IKH	TOKH	OKH	TLBO	PO	MRFO
S_1	1.60	1.40	0.50	1.80	0.20	0.10	1.20	0.90	0.10	0.20
S_2	1.50	0.70	0.50	2.80	0.10	0.50	1.20	0.30	0.40	1.10
S_3	3.00	3.40	3.40	2.00	3.40	3.40	3.00	3.20	3.40	3.20
S_4	0.10	0.70	0.10	0.40	0.10	0.10	0.90	0.10	0.10	0.20
S_5	0.70	1.60	2.80	0.40	0.60	1.90	1.00	2.50	2.40	1.30
S_6	0.90	0.70	1.10	1.00	1.00	1.00	0.90	0.90	1.10	0.90
S_7	0.60	1.00	0.20	0.40	1.20	0.40	0.90	0.80	0.30	0.40
S_8	3.40	3.40	3.40	3.40	3.40	3.40	3.20	3.40	3.40	3.40
NSA	1580.00	1580.00	1580.00	3080.00	1930.00	3100.00	6080.00	4410.00	1780.00	3030.00
Computational time (s)	0.72	0.77	0.86	1.40	0.98	1.90	1.38	2.18	0.82	1.13
Optimal value (lb)	520.66	531.48	494.30	540.05	503.38	**485.05**	529.56	501.86	487.33	493.83
Mean (lb)	590.98	558.37	530.87	571.76	549.41	**488.34**	579.05	523.36	509.75	500.76
Std (lb)	39.89	19.72	18.54	16.74	36.36	**2.59**	37.39	14.32	25.59	5.94
Increased efficiency	~	5.52%	10.17%	3.25%	7.03%	**17.37%**	2.02%	11.44%	13.74%	15.27%

2.4.4 Spatial 72-bar truss

The optimization of the 72-bar, four-level tower (Fig 2.13) was reported in [49]. The material density and modulus of elasticity of this 72-bar truss were identical to those of the 10- and 25-bar truss structures. The allowable stress of each member was ±25 ksi, and the permissible displacement of each point on the top layer in all directions was ±0.25 in. The 72-bar space truss was divided into 16 groups. Table 2.13 lists the two independent load cases applied to the spatial 72-bar space truss. The range of the discrete cross-sectional areas was 0.1–3.0 in^2 with an increment of 0.1 in^2 for each of the 16 element groups, resulting in 30 discrete cross-sections. The size of the resulting search space was $(30)^{16}$ designs.

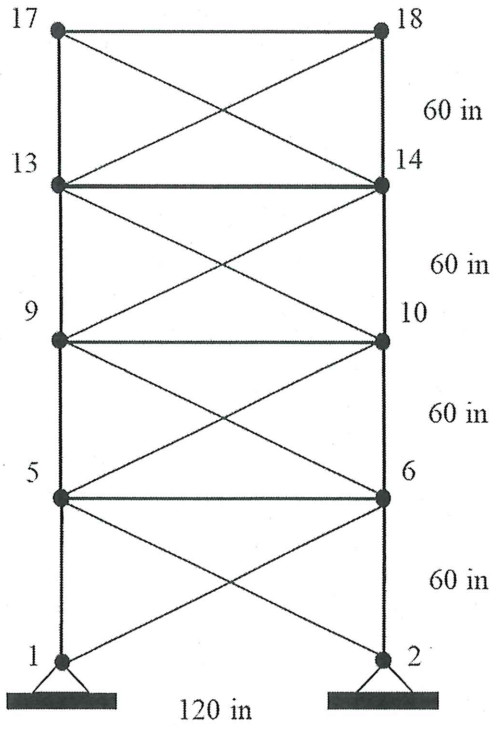

Fig 2.13a Side view

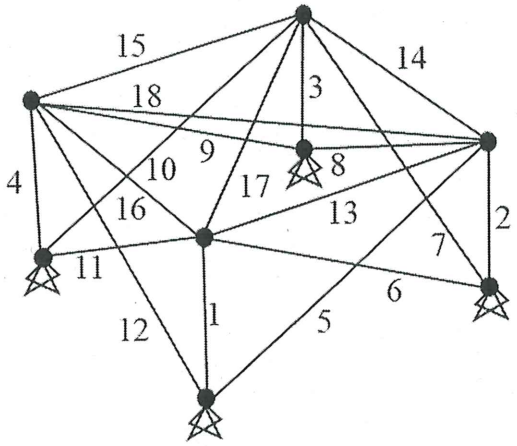

Fig 2.13b Typical story

Fig 2.13 72-bar truss

Table 2.14 compares the final optimum design and the corresponding results identified by the ten methods. The lightest weight and average weight achieved by TOKH algorithm, which are 387.94 lb and 402.30 lb, respectively. Based on the average weight of 20 independent runs, although TOKH algorithm has 1520 more structural analyses than KH, the optimization efficiency of TOKH is 53.53% higher than KH. These results indicate that

TOKH algorithm has an apparent advantage in search ability compared with the other nine methods. Fig 2.14 shows the optimization results for the spatial 72-bar truss, which is a complex structural sizing optimization problem. From Fig 2.14, different from the planar 10-bar truss as shown in Fig 2.10, the figure shows that TOKH quickly converges to a better global region in the early iterations by global exploration and continues to find the minimum in about 10-30 iterations through efficient local exploitation. MRFO algorithm still has the disadvantage of slow convergence in the early stage, and as the iterations increase, the convergence speed gradually surpasses that of TLBO and PO.

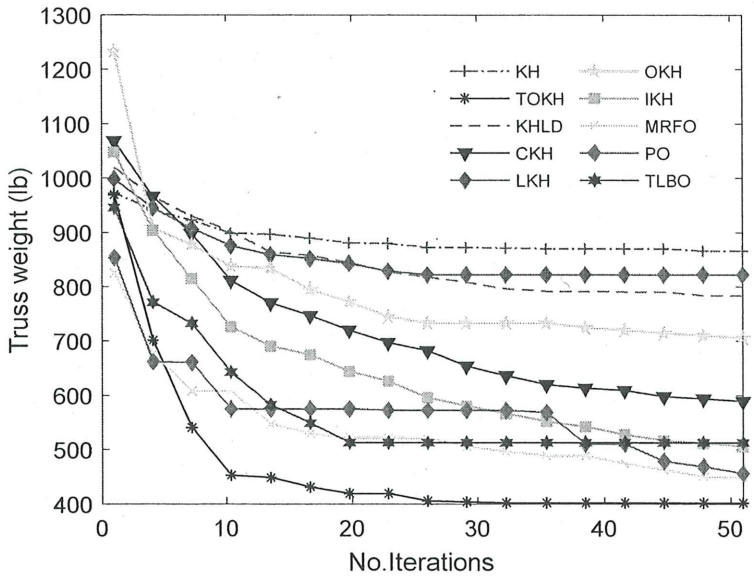

Fig 2.14 Algorithm optimization process of the 72-bar truss

Table 2.14
Optimized designs for the 72-bar truss.

	KH	KHLD	CKH	LKH	IKH	TOKH	OKH	TLBO	PO	MRFO
S_1	1.10	1.60	1.80	0.90	1.90	2.00	1.20	0.50	1.70	1.70
S_2	0.40	0.70	0.60	0.80	0.40	0.50	1.00	0.60	0.70	0.60
S_3	0.30	0.60	0.50	0.20	0.20	0.10	0.10	0.10	0.10	0.10
S_4	0.70	1.30	1.00	0.20	0.60	0.10	0.10	1.80	0.10	0.30
S_5	0.60	1.80	1.20	1.70	1.90	1.10	1.30	0.40	1.30	1.60
S_6	0.80	0.80	0.50	0.40	0.80	0.50	0.80	0.70	0.60	0.40
S_7	0.90	1.20	0.70	1.60	0.10	0.10	0.10	0.30	0.10	0.20
S_8	0.90	1.60	0.20	1.50	0.20	0.10	0.40	0.60	0.10	0.20
S_9	1.40	1.00	1.40	1.00	0.80	0.60	0.80	0.50	1.40	0.70
S_{10}	1.60	0.60	0.50	0.50	0.40	0.60	1.10	0.10	0.40	0.50
S_{11}	0.80	0.40	0.40	1.70	0.20	0.10	0.10	0.40	0.10	0.10
S_{12}	1.70	0.40	0.50	1.60	0.60	0.10	0.70	1.60	0.10	0.30
S_{13}	0.30	0.60	0.40	1.50	0.20	0.20	1.10	0.50	0.20	0.40
S_{14}	0.60	0.30	0.60	1.00	0.60	0.50	1.10	0.70	0.50	0.90
S_{15}	0.50	1.30	0.30	1.30	0.30	0.50	0.10	1.90	0.30	0.40
S_{16}	1.80	0.70	0.60	0.90	0.70	0.60	0.50	0.50	0.80	0.40
NSA	1580.00	1580.00	1580.00	3080.00	1930.00	3100.00	6080.00	4410.00	1780.00	3030.00
Computational time (s)	1.81	1.90	1.82	3.33	2.27	4.81	7.12	5.58	1.96	3.09
Optimal value (lb)	739.63	681.36	520.59	785.15	461.01	**387.94**	644.58	449.94	412.66	419.00
Mean (lb)	865.71	782.99	584.17	821.81	502.50	**402.30**	705.74	523.17	463.53	442.38
Std (lb)	67.61	65.83	49.78	33.38	24.93	**6.04**	40.20	48.81	51.43	18.21
Increased efficiency	~	9.56%	32.52%	5.07%	41.96%	**53.53%**	18.48%	39.57%	46.46%	48.90%

2.4.5 A 942-bar truss tower

The final example considered in this study is that of a 26-storey space truss tower consisting of 942 bars and 244 nodes schematically depicted in Fig 2.15. This problem aims to identify the lightest design with the design variables defined as the member cross sectional areas and divided into 59 group. A single load case is considered such that it consists of lateral loads of 5.0 KN (1.12 kips) applied in both x- and y-directions and a vertical load of –30 KN (–6.74 kips) applied in the z-direction at all nodes of the tower. The density and elastic modulus of the material are 2767.99 kg/m3 (0.1 lb/in3) and 69 GPa (1.0×10^4 ksi), respectively. The constraint conditions include allowable stresses and displacements for the truss tower. The maximum allowable stress in each member under tension and compression equals 172.37 MPa (25 ksi) while the maximum allowable displacement in x, y, z directions for the all the nodes is 38.1 cm (15.0 in). A discrete set of 137 economical standard steel sections selected from W-shape profile list based on area and radii of gyration properties is used to size the variables. The lower and upper bounds on size variables are taken as 6.16 in^2 and 215.0 in^2, respectively [50]. The size of the design search space is $(137)^{59}$. Further details regarding member grouping and design constraints can be found in reference [51].

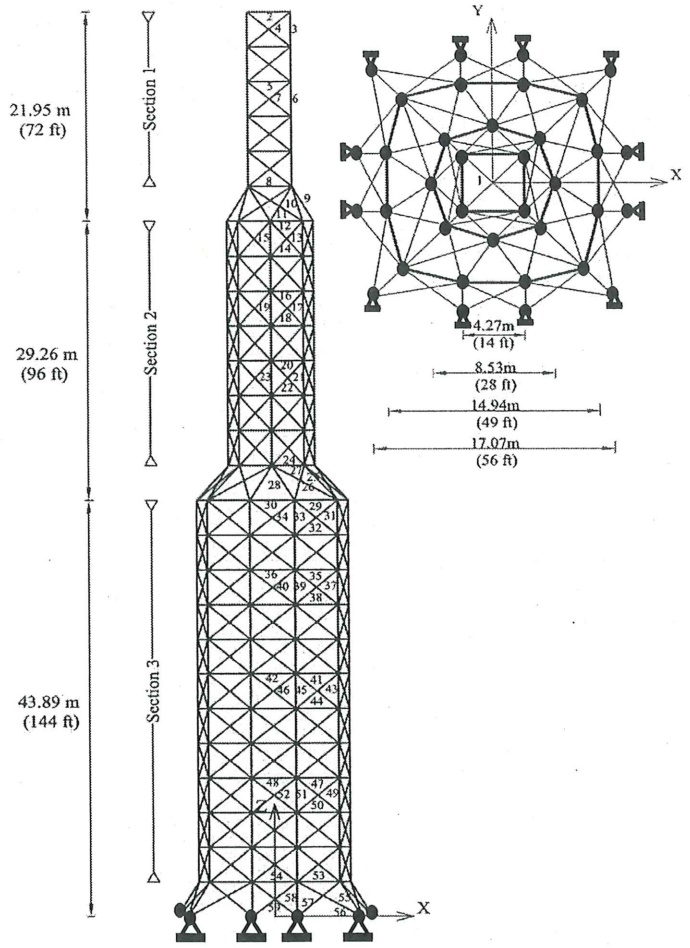

Fig 2.15 A 942-bar truss tower

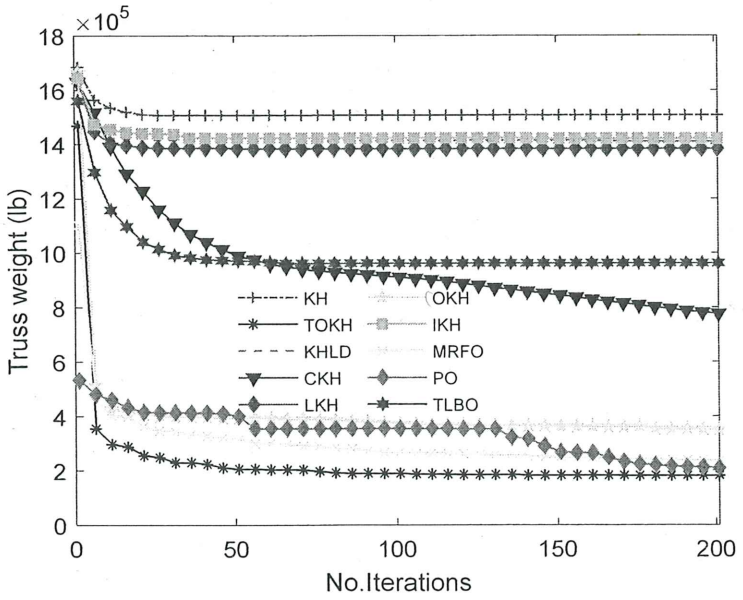

Fig 2.17 Algorithm optimization process of the 942-bar truss

Compared with the above examples, this truss tower includes more elements and load cases. Table 2.15 lists the final optimum design and the corresponding results calculated by the ten methods. Even though the lightest weight gained by TOKH algorithm is marginally heavier than PO algorithm, TOKH algorithm has the smallest average weight and standard deviation of the optimum weight among all the approaches. Regarding computational burden, due to a more discrete and nonlinear search space, TOKH requires 12,330 structural analyses and KH requires 6,230 structural analyses. Although TOKH requires a greater NSA iteration compared to KH algorithm, the truss weight is 88.01% lighter than KH. While considering both the search robustness and the optimize efficiency, the proposed achieves markedly better performance. Fig 2.17 shows the optimization process for the 942-bar truss tower, which is a complex structural sizing optimization problem with high dimensional design and nonlinear buckling constraints. When attempting to solve this optimization problem, methods may easily trap into a local optimum. Hence, a method capable of maintaining both efficient global exploration and local exploitation is likely to produce better results. As can be seen in Fig 2.17, in the early iterations, TOKH can quickly converge to a better global region by global exploration. Then, the minimum is further found in about 10-100 iterations through effective local exploitation. We can draw the conclusion that, TOKH is superior to the other algorithms during the process of optimization, while PO and MRFO performs the second and the third best in this complex truss sizing optimization, respectively.

From above-analyses about the Fig 2.10, Fig 2.12, Fig 2.14, and Fig 2.16, the intrinsic property of TOKH, which distinguishes it from the other methods in the literature, is that in optimizing the sizing of complex trusses, TOKH quickly converges to a better global region in the early iterations by global exploration, and then the local exploitation can be used to further find the minimum.

Table 2.15

Optimized designs for the 942-bar truss.

	KH	KHLD	CKH	LKH	IKH	TOKH	OKH	TLBO	PO	MRFO
S_1	17.60	17.60	101.00	38.20	35.10	6.16	23.20	59.20	31.10	11.50
S_2	48.80	20.00	18.30	42.10	38.80	6.48	11.80	91.50	6.16	16.80
S_3	16.20	32.70	51.30	61.80	17.90	6.16	20.80	51.80	7.68	15.60
S_4	68.80	21.80	50.00	15.60	83.30	6.16	9.13	48.80	6.16	7.69
S_5	8.25	15.60	6.16	6.49	17.60	6.16	11.20	35.90	6.49	13.00
S_6	8.25	25.90	118.00	10.60	20.80	6.16	14.70	147.00	10.60	9.71
S_7	178.00	19.10	56.80	6.16	18.30	8.25	10.30	6.16	6.16	8.25
S_8	196.00	24.10	7.61	10.60	12.60	6.16	9.13	162.00	6.16	14.10
S_9	26.50	68.80	35.10	101.00	32.00	27.30	25.30	32.90	13.20	29.80
S_{10}	7.08	13.30	74.10	17.90	8.25	11.20	7.61	7.08	6.16	17.10
S_{11}	14.70	101.00	83.30	88.20	20.80	7.61	23.20	6.16	6.16	9.71
S_{12}	43.20	28.20	44.70	15.80	27.30	8.84	17.90	59.20	6.16	8.25
S_{13}	44.70	55.80	38.80	8.79	31.10	6.16	38.80	6.16	6.16	14.10
S_{14}	29.80	9.71	6.16	11.50	9.13	7.69	20.80	59.20	6.16	7.08
S_{15}	44.70	15.80	81.90	26.50	6.49	8.25	7.08	117.00	6.16	14.10
S_{16}	43.20	15.80	6.16	10.60	39.90	7.08	25.30	23.20	6.16	8.85
S_{17}	61.80	50.00	109.00	19.70	18.30	6.49	31.10	74.10	13.30	11.20
S_{18}	32.90	17.90	6.16	10.00	42.70	6.16	10.60	6.16	6.16	8.85
S_{19}	35.10	88.20	125.00	35.90	21.80	6.48	11.80	162.00	6.49	11.70
S_{20}	22.60	35.90	28.50	46.70	51.30	6.16	11.20	72.80	6.16	11.80
S_{21}	42.10	35.30	38.20	6.16	44.70	20.00	10.30	53.60	31.10	14.70
S_{22}	7.69	8.79	6.16	15.60	24.10	6.16	12.60	6.16	6.16	9.12

S_{23}	162.00	11.20	74.10	13.50	14.70	8.79	14.10	80.80	6.48	16.20
S_{24}	20.80	16.70	7.08	11.80	118.00	7.08	14.10	178.00	14.10	28.20
S_{25}	7.08	17.60	22.30	15.60	17.60	23.20	13.20	178.00	29.40	29.10
S_{26}	55.80	31.10	91.50	11.20	15.60	23.20	9.71	9.71	6.16	12.60
S_{27}	61.80	83.30	55.80	8.85	14.40	9.13	12.60	18.30	6.16	21.80
S_{28}	162.00	72.80	39.90	53.60	6.16	6.16	25.30	56.80	6.48	19.70
S_{29}	98.80	31.10	6.16	15.60	8.25	6.16	21.10	89.60	7.69	13.00
S_{30}	59.20	16.20	134.00	29.10	10.60	6.16	14.70	46.70	6.16	19.70
S_{31}	44.70	10.30	50.00	25.60	19.10	35.30	18.30	178.00	31.10	20.80
S_{32}	42.10	31.20	39.90	20.00	31.10	10.30	11.20	6.16	6.16	9.71
S_{33}	13.50	16.80	6.16	11.20	14.40	6.48	31.20	62.10	6.16	14.70
S_{34}	7.61	14.40	43.20	32.00	18.30	9.71	13.50	43.20	6.16	14.70
S_{35}	26.20	23.20	125.00	10.30	31.10	7.65	9.71	14.10	6.16	12.60
S_{36}	39.90	28.50	6.16	11.80	8.25	7.08	25.30	51.80	6.16	10.00
S_{37}	29.10	18.30	17.10	32.90	18.30	39.90	24.30	15.60	31.10	39.90
S_{38}	29.80	32.90	6.49	8.79	14.10	6.16	11.20	20.00	6.16	7.08
S_{39}	35.90	21.50	16.20	11.20	8.79	6.48	27.30	125.00	6.16	10.60
S_{40}	42.10	6.49	35.90	35.90	16.80	11.80	14.70	101.00	6.16	7.69
S_{41}	19.70	11.80	20.80	26.50	11.20	6.16	9.71	28.50	6.16	8.25
S_{42}	20.80	134.00	75.90	14.40	24.10	6.16	23.20	6.16	6.49	8.25
S_{43}	22.30	25.30	59.20	28.50	42.10	48.80	35.10	125.00	51.80	32.00
S_{44}	17.10	11.50	6.16	9.13	17.60	6.16	9.71	9.71	6.16	10.60
S_{45}	44.70	32.00	14.10	16.70	8.25	6.16	44.70	80.80	6.16	9.71
S_{46}	80.80	21.50	6.16	7.69	53.60	6.16	9.12	14.70	6.16	8.25
S_{47}	21.80	7.08	6.16	23.20	12.60	7.08	7.08	101.00	6.16	17.90
S_{48}	35.10	25.30	21.80	11.80	8.79	6.48	32.90	48.80	6.16	10.00
S_{49}	46.30	38.20	68.80	48.80	28.50	65.40	39.90	51.30	75.90	35.90
S_{50}	7.69	7.69	6.16	6.48	16.20	7.08	11.50	23.20	6.16	13.20
S_{51}	29.80	59.20	25.90	22.60	16.70	6.48	10.30	6.16	6.16	11.20

S_{52}	61.80	10.60	101.00	10.60	46.30	8.25	24.10	38.20	6.49	11.80
S_{53}	10.00	20.00	35.10	14.70	21.80	10.30	32.70	196.00	16.20	11.20
S_{54}	38.80	20.80	26.20	14.70	11.20	6.48	9.71	68.80	17.90	35.10
S_{55}	19.70	72.80	162.00	26.50	38.20	31.10	27.30	162.00	31.10	26.20
S_{56}	39.90	22.60	43.20	35.90	10.00	6.16	27.30	74.10	6.16	18.30
S_{57}	62.10	51.80	6.16	31.10	74.10	55.80	29.80	17.10	32.90	29.80
S_{58}	21.50	13.50	147.00	6.16	53.60	10.30	12.60	97.90	6.16	15.60
S_{59}	215.00	32.90	38.80	16.20	31.10	6.49	9.13	107.00	6.16	9.13
NSA	6230.00	6230.00	6230.00	12230.00	7630.00	12330.00	24230.00	17910.00	7030.00	12030.00
Computational time (s)	120.11	120.64	132.06	236.92	156.79	242.04	471.50	311.18	203.98	214.48
Optimal value (lb)	7.52E5	4.47E5	6.11E5	3.29E5	4.57E5	1.70E5	2.92E5	9.09E5	**1.63E5**	2.06E5
Mean (lb)	1.51E6	1.41E6	7.75E5	1.38E6	1.42E6	**1.81E5**	3.50E5	9.63E5	2.08E5	2.33E5
Std (lb)	3.70E5	4.47E5	7.11E4	5.13E5	4.37E5	**4.70E3**	2.68E4	3.76E4	5.41E4	1.57E4
Increased efficiency	~	6.62%	48.68%	8.61%	5.97%	**88.01%**	76.82%	36.22%	86.23%	84.57%

Table 2.16

Statistical results of the optimized designs for the four trusses using different algorithms.

Example	Design Variable	KH	KHLD	CKH	LKH	IKH	TOKH	OKH	TLBO	PO	MRFO	Ranking
Planar 10-bar truss	NSA	1580.00	1580.00	1580.00	3080.00	1930.00	3100.00	6080.00	4410.00	1780.00	3030.00	8
	Computational time (s)	1.33	1.42	1.51	1.81	1.64	1.80	3.01	1.54	0.50	0.58	8
	Optimal value (lb)	5.63E3	5.83E3	5.65E3	5.78E3	5.59E3	5.49E3	6.54E3	5.49E3	5.62E3	5.49E3	1
	Mean (lb)	7.13E3	7.19E3	6.13E3	7.15E3	6.85E3	5.64E3	6.83E3	5.91E3	6.56E3	5.66E3	1
	Std (lb)	1.51E3	9.66E2	2.53E2	1.31E3	1.14E3	4.84E1	2.86E2	2.50E2	8.01E2	1.09E2	1
Spatial 25-bar truss	NSA	1580.00	1580.00	1580.00	3080.00	1930.00	3100.00	6080.00	4410.00	1780.00	3030.00	8
	Computational time (s)	0.72	0.77	0.86	1.40	0.98	1.90	1.38	2.18	0.82	1.13	8
	Optimal value (lb)	520.66	531.48	494.30	540.05	503.38	485.05	529.56	501.86	487.33	493.83	1
	Mean (lb)	590.98	558.37	530.87	571.76	549.41	488.34	579.05	523.36	509.75	500.76	1
	Std (lb)	39.89	19.72	18.54	16.74	36.36	2.59	37.39	14.32	25.59	5.94	1
Spatial 72-bar truss	NSA	1580.00	1580.00	1580.00	3080.00	1930.00	3100.00	6080.00	4410.00	1780.00	3030.00	8
	Computational time (s)	1.81	1.90	1.82	3.33	2.27	4.81	7.12	5.58	1.96	3.09	8
	Optimal value (lb)	739.63	681.36	520.59	785.15	461.01	387.94	644.58	449.94	412.66	419.00	1
	Mean (lb)	865.71	782.99	584.17	821.81	502.50	402.30	705.74	523.17	463.53	442.38	1
	Std (lb)	67.61	65.83	49.78	33.38	24.93	6.04	40.20	48.81	51.43	18.21	1
942-bar truss tower	NSA	6230.00	6230.00	6230.00	12230.00	7630.00	12330.00	24230.00	17910.00	7030.00	12030.00	8
	Computational time (s)	120.11	120.64	132.06	236.92	156.79	242.04	471.50	311.18	203.98	214.48	8
	Optimal value (lb)	7.52E5	4.47E5	6.11E5	3.29E5	4.57E5	1.70E5	2.92E5	9.09E5	1.63E5	2.06E5	2
	Mean (lb)	1.51E6	1.41E6	7.75E5	1.38E6	1.42E6	1.81E5	3.50E5	9.63E5	2.08E5	2.33E5	1
	Std (lb)	3.70E5	4.47E5	7.11E4	5.13E5	4.37E5	4.70E3	2.68E4	3.76E4	5.41E4	1.57E4	1

To examine the robustness and computational cost of TOKH, this section compares the statistical results of the four trusses examples yielded by TOKH with those gained by nine others widely used metaheuristic algorithms. Table 2.16 lists the statistical results of the optimized designs for the four truss examples from 20 runs using TLBO, PO, MRFO, KH, CKH, OKH, IKH, KHLD, LKH and TOKH. Among ten methods, TOKH identifies the lightest designs in the 10-, 25- and 72-bar trusses. As the structure becomes more complex, the performance of TOKH degrades, ranking it second in the 942-bar truss. The average weight and standard deviation obtained by TOKH ranks first among 10-, 25-, 72- and 942-bar trusses. These results indicate that TOKH possesses robustness and stability compared to the methods mentioned in the literature. Results also indicate that in the optimization of 10-, 25-, 72-, and 942-bar trusses, the optimization efficiency of TOKH algorithm has improved by 20.90, 17.37, 53.53, and 88.01%, respectively, compared to KH algorithm. With the higher the structural dimension and the stronger the discretization, the more prominent the robustness of TOKH algorithm.

However, to improve the robustness of optimized truss sizing, TOKH requires more computational cost than KH. In the 10-, 25- and 72-bar trusses, after 50 iterations, TOKH requires 3100 structural analyses while KH requires 1580 structural analyses. But considering the computational time, TOKH takes only 0.47s, 1.18s, and 3s longer than KH respectively. In the 942-bar truss, due to the higher dimensional design space, TOKH requires more structural analyses, and its computational time takes 121.93s longer than that of KH. As the truss becomes more complex, the computational cost of TOKH increases more significantly, which means that the computational efficiency is sacrificed to improve the robustness. But the computational time of TOKH increases within an acceptable range.

A novel variant of KH algorithm, referred to as TOKH algorithm, was developed for the sizing optimization of discrete truss structures. First, a crossover operator was established between the "best krill" and "suboptimal krill" to produce a robust "cross krill". Second, an ILMC operator was introduced to fine-tune the "center of food" and candidate solutions. The objective of TOKH algorithm was to optimize the balance between exploration and exploitation. Therefore, the crossover operator was used to focus on the global exploration, whereas ILMC operator was used for the local exploitation. It is found that:

1. The time complexity experiment performed using the Rastrigin benchmark function demonstrated that the running time of TOKH algorithm was linear based on the number of iterations, which was consistent with the inference of big-*O*. The two operators introduced do not change the time complexity of TOKH.
2. TOKH algorithm was compared with nine other algorithms using 15 benchmark functions. The performance of TOKH algorithm for most functions and different dimensions, particularly for different types of high-dimensional functions, was statistically superior to those of the other metaheuristic algorithms.
3. TOKH algorithm was applied to four discrete truss optimization problems under multiple loading conditions. We compared the numerical results for various trusses obtained using TOKH algorithm with other methods in the literature to verify the effectiveness, efficiency, and robustness. The results indicated that, among the ten algorithms, TOKH algorithm is competitive in terms of optimal weight, average weight, and stability. Furthermore, TOKH algorithm demonstrated significantly faster convergence to the optimal solution compared to other methods. Compared to KH algorithm, although TOKH required slightly more computational cost, its optimization efficiency improved by 20.90, 17.37, 53.53, and 88.01%, respectively. As the complexity of the truss increased, the advantage of TOKH became more evident. The proposed TOKH algorithm can serve as an ideal method for handling discrete truss problems.

Although TOKH algorithm takes on better global optimization capability, it has a high computational cost. Therefore, further research is needed on TOKH algorithm to improve robustness while reducing the computational cost.

References

[1] Kaveh, A., Talatahari, S., 2009, "A particle swarm ant colony optimization for truss structures with discrete variables," J. Constr. Steel., 65(8-9), pp. 1558-1568.

[2] Li, LJ., Huang, ZB., Liu, F., 2009, "A heuristic particle swarm optimization method for truss structures with discrete variables," Comput. Struct., 87(7-8), pp. 435-443.

[3] Gandomi, AH., Yun, GJ., Yang, XS., Talatahari, S., 2013, "Chaos-enhanced accelerated particle swarm optimization," Commun Nonlinear Sci Numer Simul., 18(2), pp. 327-340.

[4] Yang, XS., 2010, "Nature-inspired metaheuristic algorithms," Luniver press.

[5] Benzo, PG., Pereira, JM., Sena-Cruz, J., 2022, "Optimization of steel web core sandwich panel with genetic algorithm," Eng Struct., 253, p. 113805.

[6] Korus, K., Salamak, M., Jasiński, M., 2021, "Optimization of geometric parameters of arch bridges using visual programming FEM components and genetic algorithm," Eng Struct., 241, p. 112465.

[7] Khodzhaiev, M., Reuter, U., 2021, "Structural optimization of transmission towers using a novel genetic algorithm approach with a variable length genome," Eng Struct., 240, p. 112306.

[8] Simon, D., 2008, "Biogeography-based optimization," IEEE Trans. Evol. Comput., 12(6), pp. 702-713.

[9] Ergezer, M., Simon, D., Du, D., 2009, "Oppositional biogeography-based optimization," International Conference on Systems, Man and Cybernetics, IEEE., pp. 1009-1014.

[10] Du, D., Simon, D., Ergezer, M., 2009, "Biogeography-based optimization combined with evolutionary strategy and immigration refusal," International Conference on Systems, Man and Cybernetics, IEEE., pp. 997-1002.

[11] Geem, ZW., Kim, JH., Loganathan, GV., 2001, "A new heuristic optimization algorithm: harmony search," Simulation., 76(2), pp. 60-68.

[12] Murren, P., Khandelwal, K., 2014, "Design-driven harmony search (DDHS) in steel frame optimization," Eng Struct., 59, pp. 798-808.

[13] Molina-Moreno, F., García-Segura, T., Martí, JV., Yepes, V., 2017, "Optimization of buttressed earth-retaining walls using hybrid harmony search algorithms," Eng Struct., 134, pp. 205-216.

[14] Storn, R., Price, K., 1997, "Differential evolution: a simple and efficient heuristic for global optimization over continuous spaces," J Glob Optim., 11(4), pp. 341-359.

[15] Talatahari, S., Gandomi, AH., Yang, XS., Deb, S., 2015, "Optimum design of frame structures using the eagle strategy with differential evolution," Eng Struct., 91, pp. 16-25.

[16] Dorigo, M., Stutzle, T., 2004, "Ant colony optimization," MIT Press, Cambridge, MA.

[17] Eberhart, R., Kennedy, J., 1995, "A new optimizer using particle swarm theory,"

Proceedings of the sixth international symposium on micro machine and human science, IEEE., pp. 39-43.

[18] Minh, HL., Khatir, S., Wahab, MA., Cuong-Le, T., 2021, "An enhancing particle swarm optimization algorithm (EHVPSO) for damage identification in 3D transmission tower," Eng Struct., 242, p. 112412.

[19] Jiang, W., Xie, Y., Li, W., Wu, J., Long, G., 2021, "Prediction of the splitting tensile strength of the bonding interface by combining the support vector machine with the particle swarm optimization algorithm," Eng Struct., 230, p. 111696.

[20] Tapao, A., Cheerarot, R., 2017, "Optimal parameters and performance of artificial bee colony algorithm for minimum cost design of reinforced concrete frames," Eng Struct., 151, pp. 802-820.

[21] Bajer, D., Zorić, B., 2019, "An effective refined artificial bee colony algorithm for numerical optimization," Inf Sci., 504, pp. 221-275.

[22] Gorkemli, B., Karaboga, D., 2019, "A quick semantic artificial bee colony programming (qsABCP) for symbolic regression," Inf Sci., 502, pp. 346-362.

[23] Camp, CV., Farshchin, M., 2014, "Design of space trusses using modified teaching-learning based optimization," Eng Struct., 62, pp. 87-97.

[24] Shen, W., Guo, X., Wu, C., Wu, D., 2011, "Forecasting stock indices using radial basis function neural networks optimized by artificial fish swarm algorithm," Knowledge-Based Syst., 24(3), pp. 378-385.

[25] Yang, L., Qi, C., Lin, X., Li, J., Dong, X., 2019, "Prediction of dynamic increase factor for steel fibre reinforced concrete using a hybrid artificial intelligence model," Eng Struct., 189, pp. 309-318.

[26] Gandomi, AH., Yang, XS., Alavi, AH., 2011, "Mixed variable structural optimization using firefly algorithm," Comput Struct., 89(23-24), pp. 2325-2336.

[27] De Souza, RR., Miguel, LFF., Lopez, RH., Miguel, LFF., Torii, AJ., 2016, "A procedure for the size, shape and topology optimization of transmission line tower structures," Eng Struct., 111, pp. 162-184.

[28] Awad, R., 2021, "Sizing optimization of truss structures using the political optimizer (PO) algorithm," Structures., 33, pp. 4871-4894.

[29] Tran-Ngoc, H., Khatir, S., De Roeck, G., Bui-Tien, T., Wahab, MA., 2019, "An efficient artificial neural network for damage detection in bridges and beam-like

structures by improving training parameters using cuckoo search algorithm," Eng Struct., 199, p. 109637.

[30] Savković, MM., Bulatović, RR., Gašić, MM., Pavlović, GV., Stepanović, AZ., 2017, "Optimization of the box section of the main girder of the single-girder bridge crane by applying biologically inspired algorithms," Eng Struct., 148, pp. 452-465.

[31] Yang, XS., Gandomi, AH., 2012, "Bat algorithm: a novel approach for global engineering optimization," Eng Computation., 29, pp. 464-483.

[32] Bekdaş, G., Nigdeli, SM., Yang, XS., 2018, "A novel bat algorithm based optimum tuning of mass dampers for improving the seismic safety of structures," Eng Struct., 159, pp. 89-98.

[33] Cao, H., Sun, W., Chen, Y., Kong, F., Feng, L., 2023, "Sizing and shape optimization of truss employing a hybrid constraint-handling technique and manta ray foraging optimization," Expert Syst Appl., 213, p. 118999.

[34] Gandomi, AH., Alavi, AH., 2012, "Krill herd: a new bio-inspired optimization algorithm," Commun Nonlinear Sci Numer Simul., 17, pp. 4831-4845.

[35] Gandomi, AH., Talatahari, S., Tadbiri, F., Alavi. AH., 2013, "Krill herd algorithm for optimum design of truss structures," Int. J. Bio Inspired Comput., 5(5), pp. 281-288.

[36] Gandomi, AH., Alavi, AH., Talatahari, S., 2013, "Structural optimization using krill herd algorithm," Swarm intelligence and bio-inspired computation., pp. 335-349.

[37] Abdel-Basset, M., Wang, GG., Sangaiah, AK., Rushdy, E., 2019, "Krill herd algorithm based on cuckoo search for solving engineering optimization problems," Multimed. Tools Appl., 78(4), pp. 3861-3884.

[38] Wang, GG., Guo, L., Gandomi, AH., Hao, GS., Wang, H., 2014, "Chaotic krill herd algorithm," Inf Sci., 274, pp. 17-34.

[39] Wang, GG., Deb, S., Gandomi, AH., Alavi, AH., 2016, "Opposition-based krill herd algorithm with cauchy mutation and position clamping," Neurocomputing., 177, pp. 147-157.

[40] Wang, GG., Gandomi, AH., Alavi, AH., Deb, S., 2016, "A multi-stage krill herd algorithm for global numerical optimization," Int J Artif Intell Tools., 25(2), p. 1550030.

[41] Guo, L., Wang, GG., Gandomi, AH., Alavi, AH., Duan, H., 2014, "A new improved krill herd algorithm for global numerical optimization," Neurocomputing., 138, pp. 392-402.

[42] Laith, MA., Ahamad, TK., Essam, SH., 2019, "Modified krill herd algorithm for global numerical optimization problems," Advances in Nature-Inspired Computing and Applications., pp. 205-221.

[43] Li, J., Tang, Y., Hua, C., Guan, X., 2014, "An improved krill herd algorithm: krill herd with linear decreasing step," Appl Math Comput., 234(10), pp. 356-367.

[44] Wang, GG., Gandomi, AH., Alavi, AH., 2014, "Stud krill herd algorithm," Neurocomputing., 128, pp. 363-370.

[45] Wang, GG., Guo, L., Gandomi, AH., Cao, L., Alavi, AH., Duan, H., 2013, "Lévy-flight krill herd algorithm," Math Probl Eng.

[46] Lee, KS., Geem, ZW., Lee, S., Bae, KW., 2005, "The harmony search heuristic algorithm for discrete structural optimization," Eng. Optimiz., 37(7), pp. 663-684.

[47] Cheng, MY., Prayogo, D., Wu, YW., Lukito, MM., 2016, "A hybrid harmony search algorithm for discrete sizing optimization of truss structure," Autom. Constr. 69, pp. 21-33.

[48] Knuth, DE., 1976, "Big omicron and big omega and big theta," ACM Sigact News., 8(2), pp. 18-24.

[49] Camp, CV., Farshchin, M., 2014, "Design of space trusses using modified teaching-learning based optimization," Eng Struct., 62, pp. 87-97.

[50] Construction, A., 1989, "Manual of steel construction: allowable stress design," American Institute of Steel Construction: Chicago, IL, USA.

[51] Hasançebi, O., Çarbaş, S., Doğan, E., Erdal, FE., Saka, MP., 2009, "Performance evaluation of metaheuristic search techniques in the optimum design of real size pin jointed structures," Comput Struct., 87(5-6), pp. 284-302.

CHAPTER 3. OPTIMIZED PLACEMENT OF DAMPERS

3.1 Computational model of damper placement

The computational model of the optimal placement of dampers in a structure includes a structural model and an optimization model. The structural model is designed based on structural dynamics, then the corresponding optimization model is designed, and finally the optimization calculations are performed in MATLAB.

3.1.1 Structural model

Optimal damper placement requires analysis of the structural response under different damper placements, the results of which are then fed back to the algorithm for iterative optimization. The structural response can be obtained from analyzing the dynamic response of the structural story model, with the design variable being the distribution state of the dampers in each story.

In general, the output of a linear viscous damper (VD) [1-8] depends on its instantaneous relative velocity [9], that is,

$$F(t) = -c_{eq}\dot{u}(t) \tag{3.1}$$

where C_{eq} is equivalent damping coefficient, $\dot{u}(t)$ is the relative speed of the two sections of the damper. and the equation of motion for a common structural system with VDs installed are usually expressed in matrix form as

$$\begin{aligned}&[M]\{\ddot{u}(t)\} + ([C]+[C_Z])\{\dot{u}(t)\} + \\ &[K]\{u(t)\} = -[M]\{I\}\ddot{x}_g(t)\end{aligned} \tag{3.2}$$

where $\{\ddot{x}_g(t)\}$ is the ground acceleration; $[C_Z]$ is the additional damping matrix of the dampers; $[M]$, $[C]$, and $[K]$ are the mass, damping, and stiffness matrices, respectively; $\{\ddot{u}(t)\}$, $\{\dot{u}(t)\}$, and $\{u(t)\}$ are the acceleration, velocity, and displacement vectors of the main structure, respectively. Generally, the above equations are solved using classical time-history analysis methods such as the Newmark-β method and Wilson-θ method.

When the structure is subjected to external excitation, the viscous damper can effectively dissipate the energy applied to the structure by the external load, thereby reducing damage to the main body of the structure. It has many advantages, such as simple design, easy construction, good performance, etc., so it is highly popular and widely used in the construction field.

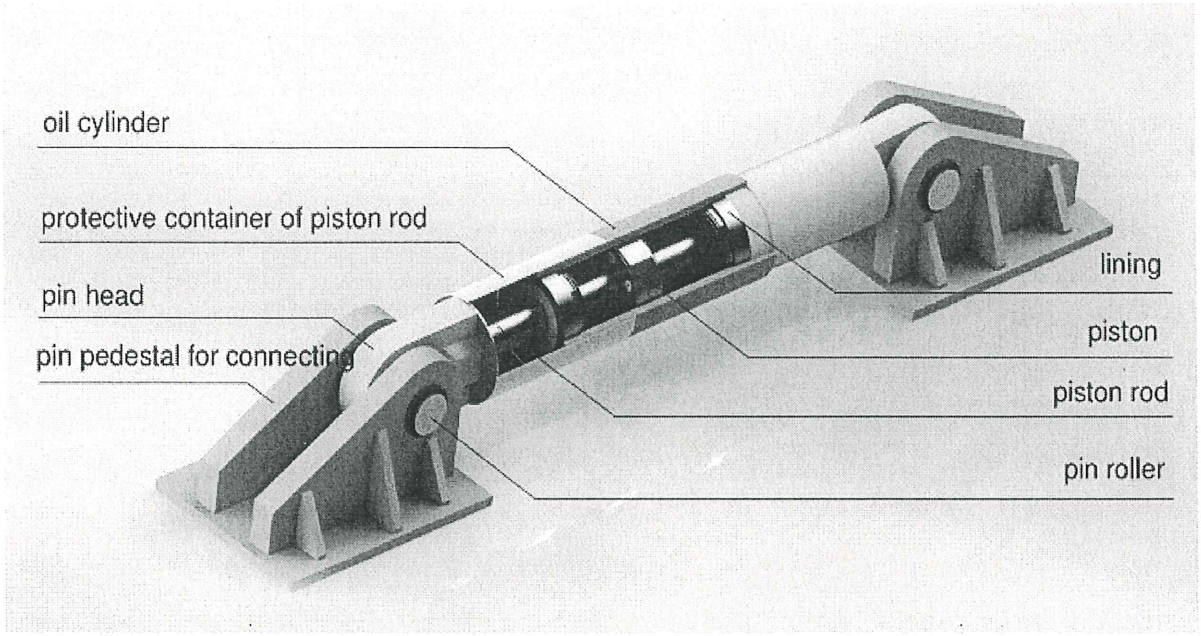

Fig. 3.1 A viscous damper

3.1.2 Optimization model

Deciding on the optimal locations of dampers in order to mitigate the dynamic response of a structural system subjected to external loadings (e.g., ground acceleration) is one of the challenges structural designers encounters. This subsection considers an optimization problem where the designer must install VDs in a structural system. The objective function denoted by $f(.)$, generally depends on the dynamic response of the structural system and the configuration and forces of the dampers, that is,

$$\begin{cases} \min f(X,t) \\ X=[x_1,\ x_2,\ ...,\ x_n]^{\mathrm{T}} \\ \text{s.t.: } x_j \in \{0,\ 1\},\ (j=1,\ 2,\ ...,\ n) \\ g(X,t) \le 0 \end{cases} \tag{3.3}$$

where n is the number of structural stories, X is the damper placement scheme, t is the time of dynamic loading, and $g\ (X,\ t) \le 0$ is a normalized constraint. In this study, the objective function f of the optimization problem is taken as the maximum inter-story drift angle [10-14].

$$f = \min(\theta_{\max}) \tag{3.4}$$

where θ is the inter-story drift angle of the structure under seismic action.

3.2 Examples

3.2.1 22-story shear structure

In this example [15] a structural designer intends to embed VDs within eight floors of a 22-story shear structure as shown in Fig. 3.2. The system is governed by Eq. (3.3), and the model's properties are given in Table 3.1. The structural damping ratio ξ is 0.05, The VD stiffness is 2.32×10^7 N/m, and the damping coefficient is 1.08×10^3 N·s/m. VDs can be installed between any two successive floors but not between the ground and the first floor. The structure is subjected to the Northridge (EW) ground acceleration [16-20], and the time-history analysis includes the first 29.9 s of the ground motion's period.

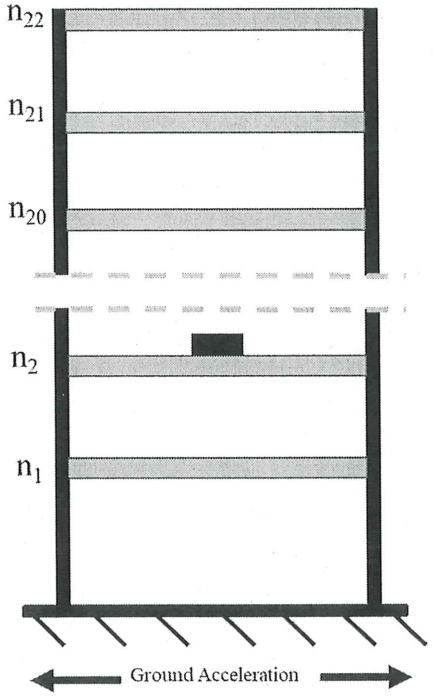

Fig. 3.2 22-story shear structure

Table 3.2 presents the optimal damper designs given by TOKH and the other metaheuristic algorithms, and as can be seen, TOKH distributed the dampers on the 2nd, 3rd, 9th–13th, and 15th stories of the structure. These metaheuristic algorithms involve the selection of random numbers, so for each optimization problem, the operation was performed ten times and then the minimum, mean, and standard deviation were calculated, as given in Table 3.2. These results clearly indicate that TOKH has considerable advantages over the other seven approaches in terms of optimal damper placement; the maximum inter-story drift angle

obtained by TOKH is 29.95×10^{-3}, which is smaller than the outcomes of the other algorithms. In term of stability, FA method has the most stable performance, followed by TOKH. It can be seen that TOKH, which does not require any gradient information, is effective in finding the optimal locations of the added VDs.

Table 3.1 Model parameters of 22-story shear structure

Floor	Story height (m)	Mass (kg)	Stiffness (N/m)
1	4.5	3.02×10^{5}	3.19×10^{8}
2	4	3.02×10^{5}	3.19×10^{8}
3-8	4	2.92×10^{5}	2.25×10^{8}
9-14	4	2.55×10^{5}	1.58×10^{8}
15-19	4	2.23×10^{5}	1.35×10^{8}

Table 3.2 Optimization results

Algorithm	Minimum	Mean	Standard deviation	Optimal placement
TOKH	29.95×10^{-3}	30.15×10^{-3}	0.10	2,3,9~13,15.
KH [21]	31.24×10^{-3}	31.60×10^{-3}	0.30	1~4,7,9~11.
ABC [22]	30.70×10^{-3}	30.97×10^{-3}	0.17	1~5,9~11.
BA [23]	31.89×10^{-3}	32.34×10^{-3}	0.33	1~7,22.
FA [24]	30.70×10^{-3}	30.76×10^{-3}	0.050	1~5,9~11.
GA [25]	30.70×10^{-3}	31.11×10^{-3}	0.29	1~5,9~11.
HS [26]	31.07×10^{-3}	32.52×10^{-3}	0.71	1~4,8~10,21.
PSO [27]	30.41×10^{-3}	31.03×10^{-3}	0.48	3,6,9~13,15.

Fig. 3.3 shows the iterative process of each algorithm. Compared to the other approaches, TOKH converges rapidly to the optimal solution, avoiding getting trapped in local optima. While PSO algorithm initially suffers from slow convergence, as the iterations proceed it gradually surpasses FA and GA, ranking second in terms of convergence rate.

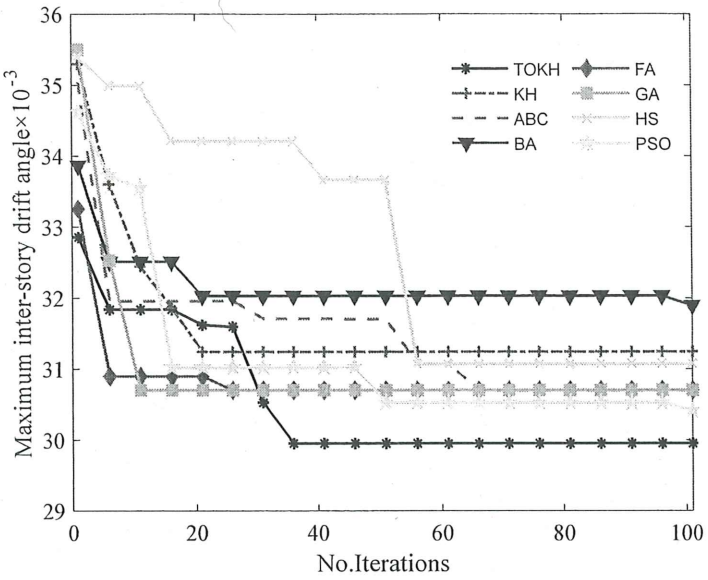

Fig. 3.3 Iterative progress of each algorithm (example 1)

3.2.2 20-story frame structure

The model used in this example is a framework structure with five spans and 20 floors taken from [28]. The intention is to install 15 VDs in spans as shown in Fig. 3.4, with only one damper allowed to be installed in each span. The properties of the structural system are summarized in Table 3.3 The damping coefficient of the VDs is 2.1×10^7 N·s/m, and the other parameters are the same as that example 1. The framework structure is subjected to EL Centro (NS) ground acceleration [29-37], with only bending and axial deformations considered, and the time-history analysis includes the first 30s.

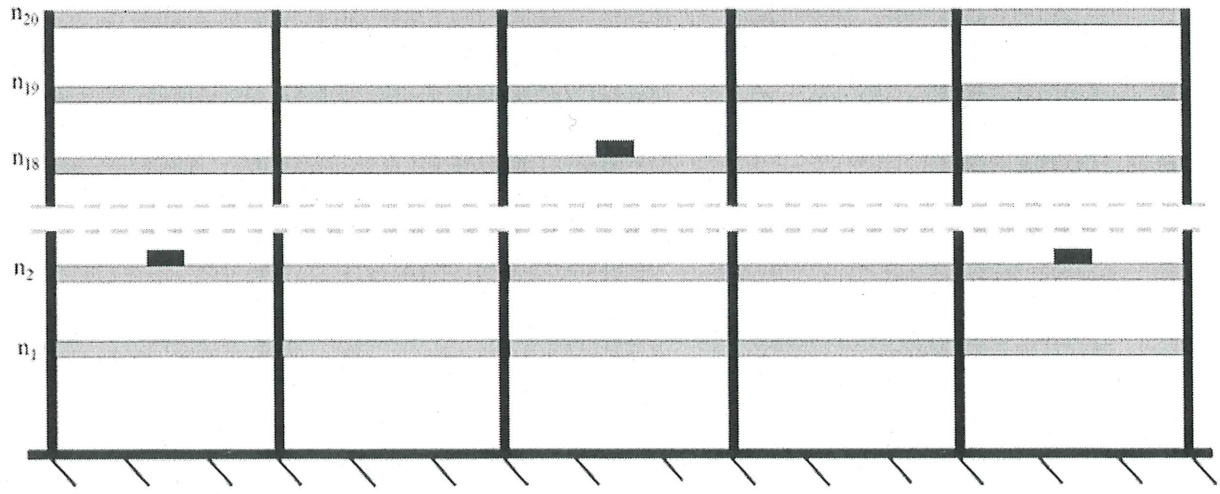

Fig. 3.4 20-story frame structure

Table 3.3 Model parameters of 20-story frame structure

Floor	Story height (m)	Mass (kg)	Stiffness (N/m)
1	3.6	3.03×10^{6}	3.19×10^{9}
2–5	3	2.92×10^{6}	2.25×10^{9}
6–10	3	2.55×10^{6}	1.58×10^{9}
11–15	3	2.23×10^{6}	1.35×10^{9}
16–20	3	2.00×10^{6}	1.30×10^{9}

Table 3.4 Optimization results under EL Centro (NS) seismic wave

Algorithm	Minimum	Mean	Standard deviation	Optimal placement
TOKH	9.34×10^{-3}	9.36×10^{-3}	5.18×10^{-3}	2(2), 3, 6(5), 7(5), 8(2)
KH	9.81×10^{-3}	9.88×10^{-3}	3.22×10^{-2}	1, 2(2), 3, 6(5), 7(2), 8(2), 10
ABC	9.37×10^{-3}	9.38×10^{-3}	1.17×10^{-3}	2,3,5,6(5), 7(5), 8, 9
BA	9.97×10^{-3}	10.08×10^{-3}	6.16×10^{-2}	3, 4(2), 5, 6(4), 7(2), 9, 11, 13(2), 17
FA	9.38×10^{-3}	9.39×10^{-3}	2.12×10^{-3}	6(5), 7(5), 8(2), 10, 11(2)
GA	9.77×10^{-3}	9.98×10^{-3}	1.72×10^{-1}	2, 6(5), 7(2), 8(2), 9(2), 10, 11
HS	9.95×10^{-3}	10.16×10^{-3}	1.33×10^{-1}	2(2), 6(4), 7, 8, 10, 13, 14, 15, 19(2), 20
PSO	9.61×10^{-3}	9.92×10^{-3}	7.79×10^{-2}	2(2), 4, 5, 6(5), 7(4), 9, 11

This example is used to study the performance of TOKH statistically to see whether it converges to an appropriate solution after a reasonable number of iterations. For this purpose, both TOKH and the other methods are executed separately 10 times each, with each execution comprising 100 iterations. The results are summarized in Table 3.4. As this table displays the best solutions found by TOKH (during separate executions) generally have lower mean value and standard deviation than those of original KH. More precisely, the distribution of the best solution found after 100 iterations by TOKH has a mean of 9.36×10^{-3} and a standard deviation of 5.18×10^{-3}, while for KH the corresponding values are 9.88×10^{-3} and 3.22×10^{-2}. This also indicates that TOKH is statistically more reliable since it has found better solutions compared to other method. The best solution found by TOKH among all of these 10 separate executions is as follows: two dampers in 2nd story, one in 3rd story, five in 6th story, five in 7th story and two in 8th story, with 9.34×10^{-3} as the corresponding value of the objective function.

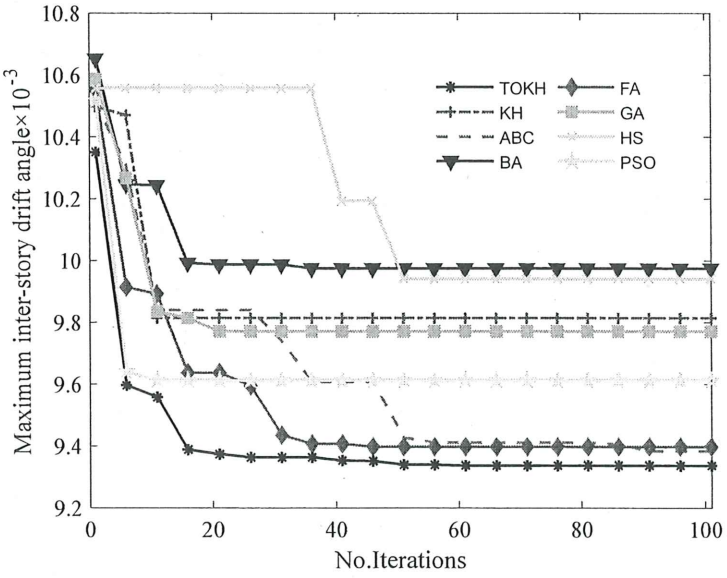

Fig. 3.5 Iterative progress of each algorithm (example 2)

Fig. 3.5 shows the convergence rates of TOKH and the other methods during 100 iterations, showcasing TOKH algorithm's persistently robust global search capability in tackling the optimal locations of dampers in structural systems. Furthermore, FA and ABC exhibit closely aligned convergence speeds and offer noteworthy performance in terms of global convergence.

3.2.3 26-story truss tower

The model used in this example is a 26-story truss tower structure [38-45]. The intention is to install 30 VDs between stories in Fig. 3.6. The properties of the structural system are summarized in Table 3.5. The damping coefficient of the VDs is 2.1×10^7 N·s/m, and the other parameters are the same as that example 1. The framework structure is subjected to Northridge (EW) ground acceleration, with only bending and axial deformations considered, and the time-history analysis includes the first 29.9s of the ground motion's period.

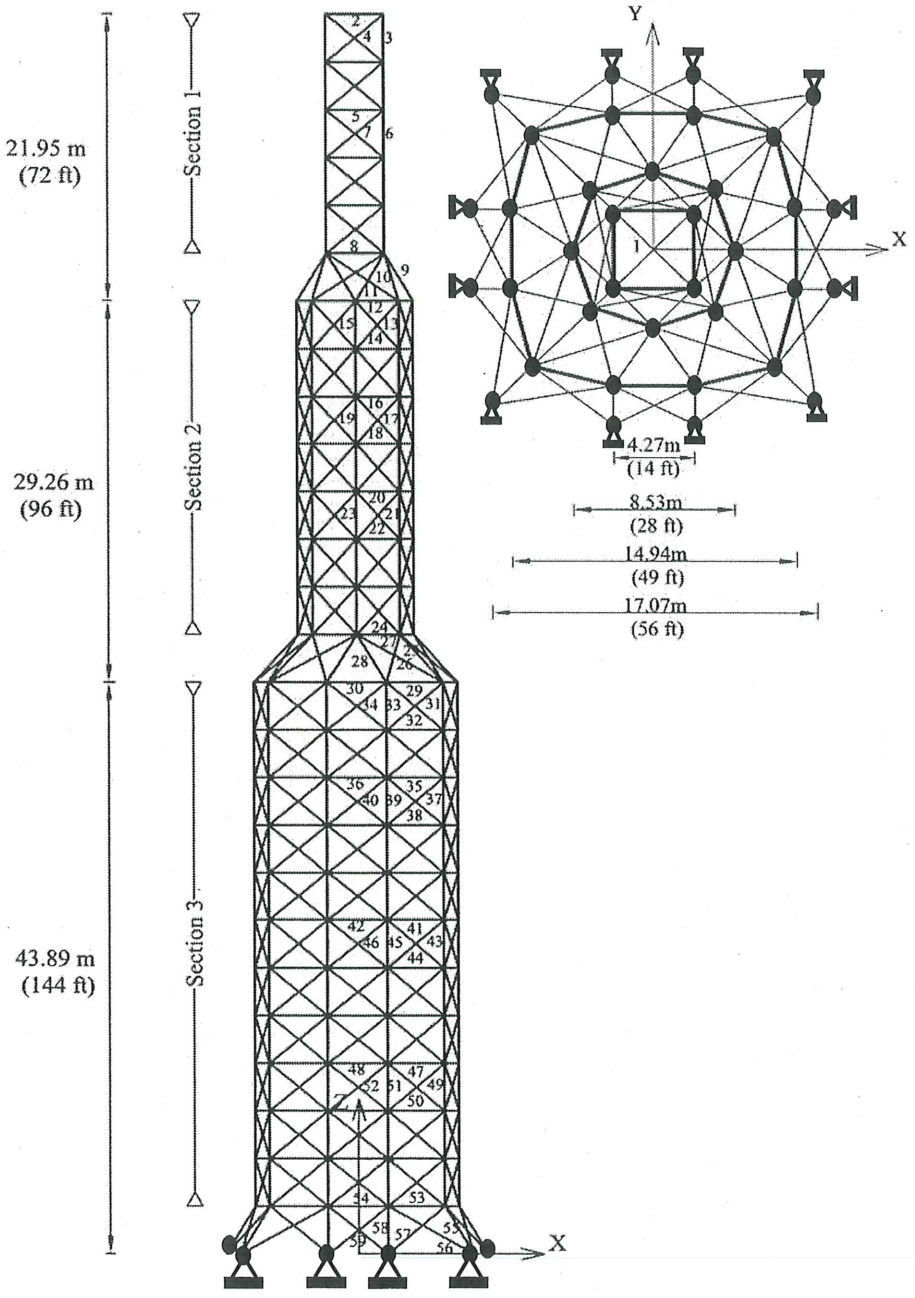

Fig. 3.6 A 942-bar truss tower

Table 3.5 Model parameters of 26-story truss tower

Floor	Story height(m)	Mass (kg)	Stiffness (N/m)
1	4.29	12.18×10^{3}	10.50×10^{6}
2 – 12	3.60	8.12×10^{3}	7.17×10^{6}
13	4.06	5.80×10^{3}	5.30×10^{6}
14 – 20	3.60	4.14×10^{3}	3.93×10^{6}
21	3.95	2.96×10^{3}	2.90×10^{6}
22 – 26	3.60	2.28×10^{3}	2.33×10^{6}

Table 3.6 presents the optimal damper designs given by TOKH and the other metaheuristic algorithms. These metaheuristic algorithms involve the selection of random numbers, so for each optimization problem, the operation was performed ten times and then the minimum, mean, and standard deviation were calculated, as given in Table 3.6. These results clearly indicate that TOKH has considerable advantages over the other seven approaches in terms of optimal damper placement; the maximum inter-story drift angle obtained by TOKH is 21.93×10^{-3}, which is smaller than the outcomes of the other algorithms. In term of stability, FA method has the most stable performance, followed by PSO.

Table 3.6 Optimization results

Algorithm	Minimum	Mean	Standard deviation	Optimal placement
TOKH	21.93×10^{-3}	22.45×10^{-3}	0.32	1(2), 2(2), 3(1), 4(1), 5(2), 6(1), 8(2), 9(1), 10(3), 11(3), 12(3), 13(3), 14(2), 15(2), 16(1), 17(1), 19(1), 20(1)
KH	22.45×10^{-3}	23.15×10^{-3}	0.67	1(2), 2(3), 3(2), 4(1), 5(1), 6(1), 7(2), 8(2), 9(2), 11(2), 12(1), 13(2), 14(2), 15(2), 16(1), 17(2), 18(1), 19(1)
ABC	22.59×10^{-3}	23.02×10^{-3}	0.27	1(8), 2(1), 3(1), 5(1), 7(1), 8(2), 9(1), 11(2), 12(1), 13(1), 14(2), 15(2), 16(2), 17(2), 18(1), 22(2)
BA	23.12×10^{-3}	24.62×10^{-3}	0.80	1(2), 2(2), 3(2), 4(1), 5(2), 6(1),

				8(1), 9(1), 10(2), 11(2), 12(2), 13(1), 14(2), 15(1), 16(1), 17(1), 18(1), 19(1), 20(1), 21(1), 22(1), 23(1), 25(1)
FA	23.52×10^{-3}	23.78×10^{-3}	0.11	2(1), 3(1), 4(1), 5(3), 6(1), 7(1), 8(3), 9(2), 10(1), 11(2), 12(3), 13(1), 14(2), 15(3), 16(2), 17(1), 18(1), 20(1)
GA	24.19×10^{-3}	24.95×10^{-3}	0.69	1(6), 2(2), 3(1), 5(1), 6(2), 7(2), 8(3), 9(1), 10(1), 11(2), 12(1), 13(1), 14(2), 15(2), 16(2), 17(1), 18(1)
HS	23.68×10^{-3}	24.57×10^{-3}	0.49	2(2), 3(2), 8(2), 9(3), 10(3), 11(1), 13(1), 14(4), 15(1), 16(1), 17(2), 18(1), 20(1), 22(1), 24(1), 25(2), 26(2)
PSO	22.19×10^{-3}	22.65×10^{-3}	0.22	2(1), 4(1), 5(2), 6(1), 8(2), 9(2), 10(1), 11(2), 12(1), 13(2), 14(4), 15(2), 16(2), 17(1), 18(2), 19(1), 20(4)

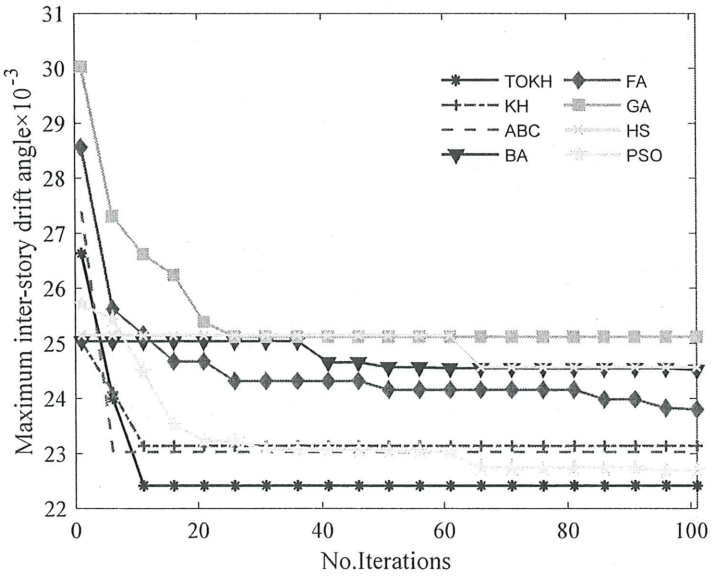

Fig. 3.7 Iterative progress of each algorithm (example 3)

Fig. 3.7 shows the convergence rates of TOKH and the other methods during 100 iterations. From Fig. 3.7, we can draw the conclusion that, TOKH is significantly superior to the other algorithms during the process of optimization, while PSO and ABC performs the second and the third best in this constrained optimization problem, respectively.

This study proposes the TOKH algorithm for finding the optimal locations of dampers in a structural system and in particular for a high-rise structure. It is found that:

1. The two high-rise structural examples indicate that compared with other algorithms, the VD locations found by TOKH algorithm give better seismic performance. Meanwhile, the TOKH also has good global convergence.

2. The VD placements obtained by TOKH are mainly in the middle and lower stories of the high-rise structure, which is consistent with practical experience.

3. TOKH offers a practical and powerful method for determining the optimal damper placement in high-rise structures.

Looking to the future, the expectation is that TOKH will be extended to optimization analysis of the elastic–plastic phase of structures, and subsequent research will be focused on that aspect.

References

[1] Lee D, Taylor D P. Viscous damper development and future trends. The structural design of tall buildings, 2001, 10(5): 311-320.

[2] Whittle J K, Williams M S, Karavasilis T L, et al. A comparison of viscous damper placement methods for improving seismic building design. Journal of Earthquake Engineering, 2012, 16(4): 540-560.

[3] Pekcan G, Mander J B, Chen S S. Fundamental considerations for the design of non-linear viscous dampers. Earthquake engineering & structural dynamics, 1999, 28(11): 1405-1425.

[4] De Domenico D, Ricciardi G, Takewaki I. Design strategies of viscous dampers for seismic protection of building structures: a review. Soil dynamics and earthquake engineering, 2019, 118: 144-165.

[5] Main J A, Jones N P. Free vibrations of taut cable with attached damper. I: Linear viscous damper. Journal of Engineering Mechanics, 2002, 128(10): 1062-1071.

[6] Makris N, Constantinou M C. Spring-viscous damper systems for combined seismic and

vibration isolation. Earthquake engineering & structural dynamics, 1992, 21(8): 649-664.

[7] Mcnamara R J, Taylor D P. Fluid viscous dampers for high-rise buildings. The structural design of tall and special buildings, 2003, 12(2): 145-154.

[8] Priestley M J N, Grant D N. Viscous damping in seismic design and analysis. Journal of earthquake engineering, 2005, 9(spec02): 229-255.

[9] J.Tedesco, W.G.McDougal, and C.A.Ross: Structural dynamics, London, UK, Pearson Education, 2000.

[10] Cai J, Bu G, Yang C, et al. Calculation methods for inter-story drifts of building structures. Advances in Structural Engineering, 2014, 17(5): 735-745.

[11] Çolak H, Türker H T, Coşkun H. Accurate Estimation of Inter-Story Drift Ratio in Multistory Framed Buildings Using a Novel Continuous Beam Model. Applied Sciences, 2023, 13(13): 7819.

[12] Chang C Y, Huang C W. Non-contact measurement of inter-story drift in three-layer RC structure under seismic vibration using digital image correlation. Mechanical Systems and Signal Processing, 2020, 136: 106500.

[13] Wang W, Zou C, Chen Y, et al. Seismic design of multistory tension-only concentrically braced beam-through frames aimed at uniform inter-story drift[J]. Journal of Constructional Steel Research, 2016, 122: 326-338.

[14] Fu J Y, Zheng Q X, Wu J R, et al. Wind-induced inter-story drift analysis and equivalent static wind load for multiple targets of tall buildings. The Structural Design of Tall and Special Buildings, 2016, 25(6): 297-321.

[15] Kookalani S, Shen D, Zhu L L, et al. An overview of optimal damper placement methods in structures. Iranian Journal of Science and Technology, Transactions of Civil Engineering, 2022: 1-20.

[16] Boatwright J, Thywissen K, Seekins L C. Correlation of ground motion and intensity for the 17 January 1994 Northridge, California, earthquake. Bulletin of the Seismological Society of America, 2001, 91(4): 739-752.

[17] Su F, Anderson J G, Zeng Y. Study of weak and strong ground motion including nonlinearity from the Northridge, California, earthquake sequence. Bulletin of the Seismological Society of America, 1998, 88(6): 1411-1425.

[18] Shakal A F, Huang M J, Darragh R B. Interpretation of significant ground-response and structure strong motions recorded during the 1994 Northridge earthquake. Bulletin of the

Seismological Society of America, 1996, 86(1B): S231-S246.

[19] Nagarajaiah S, Xiaohong S. Response of base-isolated USC hospital building in Northridge earthquake. Journal of structural engineering, 2000, 126(10): 1177-1186.

[20] Bardet J P, Davis C. Engineering observations on ground motion at the Van Norman Complex after the 1994 Northridge earthquake. Bulletin of the seismological Society of America, 1996, 86(1B): S333-S349.

[21] Gandomi A H, Alavi A H. Krill herd: a new bio-inspired optimization algorithm. Communications in nonlinear science and numerical simulation, 2012, 17(12): 4831-4845.

[22] Karaboga D, Basturk B. On the performance of artificial bee colony (ABC) algorithm. Applied soft computing, 2008, 8(1): 687-697.

[23] Talal R. Comparative study between the (ba) algorithm and (pso) algorithm to train (rbf) network at data classification. International Journal of Computer Applications, 2014, 92(5): 16-22.

[24] Tan Y, Zhu Y. Fireworks algorithm for optimization//Advances in Swarm Intelligence: First International Conference, ICSI 2010, Beijing, China, June 12-15, 2010, Proceedings, Part I 1. Springer Berlin Heidelberg, 2010: 355-364.

[25] Dasgupta K, Mandal B, Dutta P, et al. A genetic algorithm (ga) based load balancing strategy for cloud computing. Procedia Technology, 2013, 10: 340-347.

[26] Yang X S. Harmony search as a metaheuristic algorithm. Music-inspired harmony search algorithm: theory and applications, 2009: 1-14.

[27] De Oca M A M, Stutzle T, Birattari M, et al. Frankenstein's PSO: a composite particle swarm optimization algorithm. IEEE Transactions on Evolutionary Computation, 2009, 13(5): 1120-1132.

[28] Ohtori,Y., Christenson, R.E., Spencer Jr, B.F., and Dyke, S.J., 2004, Benchmark control problems for seismically excited nonlinear buildings, Journal of engineering mechanics., 130, pp.366-385.

[29] Udwadia F E, Trifunac M D. Comparison of earthquake and microtremor ground motions in El Centro, California. Bulletin of the Seismological Society of America, 1973, 63(4): 1227-1253.

[30] Niazi M. Inferred displacements, velocities and rotations of a long rigid foundation located at El Centro differential array site during the 1979 Imperial Valley, California,

earthquake. Earthquake engineering & structural dynamics, 1986, 14(4): 531-542.

[31] Orabi I I, Ahmadi G. Horizontal-vertical Response Spectra for El Centro (1940) Earthquake. Department of Mechanical and Industrial Engineering, Clarkson University, 1985.

[32] Shoemaker J M. Acceleration Response of Rigid and Flexible Nonstructural Components in Building Subjected to Strong Ground Motions. 2010.

[33] Chen Q, Yuan W, Li Y, et al. Dynamic response characteristics of super high-rise buildings subjected to long-period ground motions. Journal of Central South University, 2013, 20(5): 1341-1353.

[34] McGuire R K. A simple model for estimating Fourier amplitude spectra of horizontal ground acceleration. Bulletin of the Seismological Society of America, 1978, 68(3): 803-822.

[35] You B, Lee J H, Ku K H. Evaluation of seismic acceleration responses of base-isolated and nonisolated structures varying with mechanical characteristics of foundations. 1996.

[36] Taghavi S, Miranda E. Approximate floor acceleration demands in multistory buildings. II: Applications. Journal of Structural Engineering, 2005, 131(2): 212-220.

[37] Gao X, Ling X, Tang L, et al. Soil–pile-bridge structure interaction in liquefying ground using shake table testing. Soil Dynamics and Earthquake Engineering, 2011, 31(7): 1009-1017.

[38] Stolpe M. Truss optimization with discrete design variables: a critical review. Structural and Multidisciplinary Optimization, 2016, 53: 349-374.

[39] Gomes H M. Truss optimization with dynamic constraints using a particle swarm algorithm. Expert Systems with Applications, 2011, 38(1): 957-968.

[40] Wang D, Zhang W H, Jiang J S. Truss shape optimization with multiple displacement constraints. Computer methods in applied mechanics and engineering, 2002, 191(33): 3597-3612.

[41] Martinez P, Marti P, Querin O M. Growth method for size, topology, and geometry optimization of truss structures. Structural and Multidisciplinary Optimization, 2007, 33: 13-26.

[42] Miguel L F F, Miguel L F F. Shape and size optimization of truss structures considering dynamic constraints through modern metaheuristic algorithms. Expert Systems with Applications, 2012, 39(10): 9458-9467.

[43] Tang W, Tong L, Gu Y. Improved genetic algorithm for design optimization of truss structures with sizing, shape and topology variables. International Journal for Numerical Methods in Engineering, 2005, 62(13): 1737-1762.

[44] Lingyun W, Mei Z, Guangming W, et al. Truss optimization on shape and sizing with frequency constraints based on genetic algorithm. Computational Mechanics, 2005, 35: 361-368.

[45] Krishnamoorthy C S, Prasanna Venkatesh P, Sudarshan R. Object-oriented framework for genetic algorithms with application to space truss optimization. Journal of computing in civil engineering, 2002, 16(1): 66-75.

CHAPTER 4. CONCLUSIONS

In this research, a target-oriented krill herd (TOKH) algorithm is proposed to solve practical engineering optimization, especially the optimal placement of dampers in high-rise structures.

In terms of truss structure size optimization:

1. The time complexity experiment performed using the Rastrigin benchmark function demonstrated that the running time of TOKH algorithm was linear based on the number of iterations, which was consistent with the inference of big-O. The two operators introduced do not change the time complexity of TOKH.

2. TOKH algorithm was compared with nine other algorithms using 15 benchmark functions. The performance of TOKH algorithm for most functions and different dimensions, particularly for different types of high-dimensional functions, was statistically superior to those of the other metaheuristic algorithms.

3. TOKH algorithm was applied to four discrete truss optimization problems under multiple loading conditions. We compared the numerical results for various trusses obtained using TOKH algorithm with other methods in the literature to verify the effectiveness, efficiency, and robustness. The results indicated that, among the ten algorithms, TOKH algorithm is competitive in terms of optimal weight, average weight, and stability. Furthermore, TOKH algorithm demonstrated significantly faster convergence to the optimal solution compared to other methods. Compared to KH algorithm, although TOKH required slightly more computational cost, its optimization efficiency improved by 20.90, 17.37, 53.53, and 88.01%, respectively. As the complexity of the truss increased, the advantage of TOKH became more evident. The proposed TOKH algorithm can serve as an ideal method for handling discrete truss problems.

In terms of optimal damper placement in high-rise structures:

1: The high-rise structural example indicate that compared with other algorithms, the VD locations found by TOKH algorithm give better seismic performance. Meanwhile, the TOKH also has good global convergence.

2: The VD placements obtained by TOKH are mainly in the middle and lower stories of the high-rise structure, which is consistent with practical experience.

3: TOKH offers a practical and powerful method for determining the optimal damper

placement in high-rise structures.

In the future, in-depth research should be continued from the following aspects.

1: Although TOKH algorithm takes on better global optimization capability, it has a high computational cost. Therefore, further research is needed on TOKH algorithm to improve robustness while reducing the computational cost.

2: Future trends should focus on enhancing the structural optimization performance of the TOKH algorithm, and further work into the continuation and applications of the proposed technique, like, in combination with boundary update approach for optimization problems of implicit constraints.

3: TOKH has a high computational cost in engineering optimization. Further research is needed on TOKH to improve robustness while reducing the computational cost.

4: At present, the structure under earthquake is all elastic deformation, and the structural plastic deformation needs to be further considered.

LIST OF PUBLICATIONS

Journal papers

[1]. Lixiang Cheng, Yan-Gang Zhao, Pei-Pei Li, and Lewei Yan. Sizing and shape optimization of discrete truss employing a target-oriented krill herd algorithm. ASCE-ASME Journal of Risk and Uncertainty in Engineering Systems Part B: Mechanical Engineering. 2023. (Accept)

[2]. Lixiang Cheng, Yan-Gang Zhao, and Lewei Yan. A cooperative and competitive krill herd algorithm for structural optimization. Engineering Optimization. (Under revision)

[3]. Lixiang Cheng, Yan-Gang Zhao. Optimal placement of dampers in structures using target-oriented krill herd algorithm. Journal of Structural Engineering. B. (Under review)

Conference papers

[1]. Lixiang Cheng, Yan-Gang Zhao. Structural reliability analysis using latin hypercube sampling particle swarm optimization algorithm. ICOSSAR2022.

[2] Lixiang Cheng, Yan-Gang Zhao. Structural reliability analysis using improved krill herd algorithm. 29th International European Safety and Reliability Conference.

[3] Lixiang Cheng. Structural reliability analysis using cooperative and competitive krill herd algorithm. CoEEPE 2023.

[4] Lixiang Cheng, Yan-Gang Zhao. Structural reliability analysis using information exchange particle swarm optimization algorithm. IFRERM2023.

[5] Lixiang Cheng, Yan-Gang Zhao. Structural reliability analysis using improved particle swarm optimization algorithm. Summaries of Technical Papers of Annual Meeting, AIJ 2023. pp. 1-2.

[6] Lixiang Cheng, Yan-Gang Zhao. A structural reliability analysis method based on local mutation crossover krill herd algorithm. Summaries of Technical Papers of Annual Meeting, AIJ 2022. pp. 5-6.

[7] Lixiang Cheng, Yan-Gang Zhao. A structural reliability analysis method based on target-oriented krill herd algorithm. Summaries of Technical Papers of Annual Meeting, AIJ 2021. pp. 15-16.

ACKNOWLEDGMENTS

I extend my deepest gratitude to my advisor, Professor Yan-gang Zhao, whose expertise and understanding added considerably to my research experience. His guidance and mentorship were paramount not only to this dissertation but also to shaping my academic and professional journey. It is great honor to work with him and I would keep those things I have learned in mind and take them as my guideline for my future work.

At the same time, I am very grateful to Professor Shimazaki, Associate Professor Haizhong Zhang and Assistant Professor Shirai for helping me with my life, allowing me to concentrate on my research. They gave me a lot of useful help in solving the met difficulties. Without their patient help, it is almost impossible for me to get used to the life in Japan so smoothly.

Great thanks go to the review committee members: Professor Kazushi Shimazaki, Professor Enomoto Takahisa, Professor Fujita Masanori and Professor Yoshie Keisuke for their valuable comments and suggestions on this work.

Sincere thanks go to the members of Zhao laboratory for their help in solving the met difficulties in life, work, and study, etc. Thanks for becoming of my good friends in this foreign country.

Finally, I would like to thank my girlfriend and family for their loves and support. Without their constant encouragement and support, I could not have completed my PhD studies so smoothly.

Lixiang Cheng

January 2024 in Yokohama